

University of Alberta

Particle Contributions to Kinematic Friction in Slurry Pipeline Flow

by

Daniel Peter Gillies

A thesis submitted to the Faculty of Graduate Studies and Research
in partial fulfillment of the requirements for the degree of

Master of Science

in

Chemical Engineering

Department of Chemical and Materials Engineering

©Daniel Peter Gillies
Spring 2013
Edmonton, Alberta

Permission is hereby granted to the University of Alberta Libraries to reproduce single copies of this thesis and to lend or sell such copies for private, scholarly or scientific research purposes only. Where the thesis is converted to, or otherwise made available in digital form, the University of Alberta will advise potential users of the thesis of these terms.

The author reserves all other publication and other rights in association with the copyright in the thesis and, except as herein before provided, neither the thesis nor any substantial portion thereof may be printed or otherwise reproduced in any material form whatsoever without the author's prior written permission.

ABSTRACT

In this research, two areas important to the analysis and prediction of slurry friction losses during pipeline flow were studied. A correlation was developed to predict the particle friction factor, f_s , for prediction of the kinematic friction loss component of slurry friction losses. Methods for determining the maximum particle concentration, C_∞ were studied and compared.

Slurries of four particle types: aluminum oxide, petroleum coke, angular sand, and silica flour in water were tested in a 75 mm diameter pipeline loop at different concentrations. These particles were chosen in order to study the effects of particle density and particle size on the kinematic friction loss component of slurry friction losses.

Experiments where pressure loss was measured as a function of velocity were conducted and the data collected were used, along with data previously collected by researchers at the SRC Pipe Flow Technology Centre, to create a new f_s correlation. The correlation is logarithmic and covers a wider range of dimensionless particle diameters (d^+) than previous correlations.

Four methods were studied for determining C_∞ : pipeline loop tests, concentric cylinder viscometer tests, settled bed tests, and a semi-empirical correlation. It is recommended that the pipeline method be used to get very accurate predictions of C_∞ . If pipeline tests cannot be conducted, the settled bed tests and the Hoffmann-Finkers correlation had the least error. The viscometer method is not

recommended due to its inability to accurately predict C_∞ for particles other than angular sand.

Future work should be performed to expand the new f_s correlation for complex slurries containing particles with broad or multimodal size distributions and slurries containing particles with different densities.

ACKNOWLEDGEMENTS

I am indebted to Dr. Randy Gillies for his patience and guidance during the experimental testing and the analysis of results.

I would like to thank the Saskatchewan Research Council for providing a pipe loop, the laboratories and office space during my research. Also, I would like to thank the employees of the SRC Pipe Flow Technology Centre for their assistance with my laboratory experiments, with running and maintaining the 75 mm pipeline loop, and for all the laughs we shared at coffee and lunch time. I give thanks to R. Sun, P.Schergevitch, Dr. M. McKibben, C. Knops, D.Riley, Dr. R. Spelay, M. Skoretz, D. Zacharias, L. McGilp, and J. Fenez.

Financial support from Canada's Natural Sciences and Engineering Research Council (NSERC) and from the sponsoring companies of the NSERC Industrial Research Chair in Pipeline Transport Processes is gratefully acknowledged.

I would like to thank Dr. Sean Sanders for taking me on as a graduate student at the University of Alberta. I must thank him for his invaluable guidance during my graduate courses in Edmonton as well as for allowing me to spend the majority of my time at home in Saskatoon performing my research. Dr. Sean Sanders is one of the busiest people I know, with many graduate students and other commitments, yet whenever I needed assistance he was always available to help.

Finally, thank you to my friends and family for their love and support.

TABLE OF CONTENTS

ABSTRACT

ACKNOWLEDGEMENTS

TABLE OF CONTENTS

LIST OF TABLES

LIST OF FIGURES

1	INTRODUCTION	1
2	THEORY	4
3	EQUIPMENT, MATERIALS & PROCEDURES	19
3.1	<i>Pipeline Loop</i>	19
3.2	<i>Pipeline Test Procedure</i>	21
3.3	<i>Laboratory Tests</i>	26
3.3.1	Concentric Cylinder Viscometer Tests to Determine C_{∞}	26
3.3.2	Particle density determination	28
3.3.3	Particle Size Determination	29
3.3.4	Settling Tests to Determine C_{∞}	33
4	RESULTS AND DISCUSSION	35
4.1	<i>Particle Characterization</i>	35
4.2	<i>Pipeline Tests</i>	41
4.2.1	Overview	41
4.2.2	Determining C_{∞}	42

4.2.3	Developing an improved correlation for f_s	44
4.3	<i>Alternate Methods for Determining C_∞</i>	47
4.3.1	Concentric Cylinder Viscometer Tests	47
4.3.2	Settling Tests	49
4.3.3	Predictions of C_∞ using the Hoffmann & Finkers' correlation	50
4.3.4	Summary of Methods	51
4.4	<i>Bimodal distributions of different particle types</i>	54
5	CONCLUSIONS AND RECOMMENDATIONS	57
6	REFERENCES	60
	SYMBOLS	64
	APPENDICES	68
	<i>Appendix A: Particle Size Distributions</i>	69
	<i>Appendix B: Viscometer Sample Calculation and Data</i>	70
	<i>Appendix C: Experimental Pipeline Pressure Gradients</i>	77
	<i>Appendix D: Rejected Model Fits</i>	84

LIST OF TABLES

Table 4.1 Properties of particles used in this study	41
Table 4.2 C_{∞} values determined from pipeline tests.....	43
Table 4.3 Maximum packing concentration values determined from the Schaan correlation ..	48
Table 4.4 Maximum packing concentration values determined from settling tests	49
Table 4.5 C_{∞} values found using different methods.....	50
Table 4.6 Comparison of methods for determining C_{∞} for petroleum coke	53

LIST OF FIGURES

Figure 2.1 A comparison of experimentally determined friction factors for 92 μm sand-in-water slurries with expected friction factors obtained using the slurry viscosity method.	9
Figure 2.2 A comparison of experimentally determined friction factors for 92 μm sand-in-water slurries flowing in a 50 mm pipe with expected friction factors obtained using the pseudo-fluid slurry approximation.	10
Figure 2.3 A comparison of the predictions of the Shook correlation and experimental data for pipeline flow of 92 μm sand-in-water slurries.....	17
Figure 3.1 75 mm pipeline loop and instrumentation.....	19
Figure 3.2 Gamma ray densitometer; pipe diameter is D.	24
Figure 3.3 Concentric Cylinder Viscometer	27
Figure 3.4 Andreasen pipette.....	31
Figure 4.1 Photograph of aluminum oxide particles	36
Figure 4.2 Photograph of angular sand particles (Lane Mountain 125).....	37
Figure 4.3 Photograph of silica flour particles (SIL 325)	38
Figure 4.4 Photograph of petroleum coke particles.....	39
Figure 4.5 Particle size distributions.....	40
Figure 4.6 Determining C_{∞} for aluminum oxide slurries from 75 mm pipeline tests using a logarithmic regression function	43
Figure 4.7 Logarithmic relationship describing kinematic friction behavior of different particle slurries.....	45
Figure 4.8 Schaan's correlation (solid line) and experimental data points for concentric cylinder viscometer tests of aluminum oxide slurries.....	48
Figure 4.9 Friction loss predictions for an aluminum oxide slurry (30% solids by volume) in a 75 mm pipeline loop. Predictions shown here based on the different methods for prediction C_{∞} . Actual pipeline data shown for comparison.....	52

**Figure 4.10 Bimodal particle slurries compared with the kinematic friction correlation for single
particle slurries 56**

1 INTRODUCTION

Slurry pipelines are widely used in many industries including mining, mineral processing, drilling, food processing and nuclear waste handling.

Slurry pipelines are very important to Canadian industry and, over the years, Canadian researchers have made very significant research and development contributions in the area. A Saskatoon based group composed of Professor Clifton Shook of the University of Saskatchewan and his colleagues at the Saskatchewan Research Council (SRC) started a slurry pipelining research program in 1960. While Dr. Shook is now deceased, the SRC continues to operate a slurry pipelining R&D lab in Saskatoon. A Queen's University group led by Professor Kenneth Wilson was actively involved in slurry pipelining research for about three decades starting in the 1970's. Recently, an NSERC Industrial Chair in the area of Pipeline Transport Processes was established at the University of Alberta. The continued development of slurry pipelining technology is a focal area for the University of Alberta group.

Slurries are typically classified as homogeneous or heterogeneous. In homogenous slurries the concentration of particles across the pipeline cross-section is uniform while in heterogeneous slurries the concentration distribution is not uniform. The homogeneous slurry classification tends to apply only when the particles are small and flocculating, e.g. clay particles. Slurries often are treated as heterogeneous when the non-flocculating particles are of greater density than the

carrying liquid and the turbulent forces in the flow are not strong enough to fully suspend all particles.

Designers of slurry pipelines are required to predict the pressure required to maintain the desired flow in the pipeline. For steady state pipeline operation, the pressure requirement is dependent on gravitational effects and on the friction losses accompanying the flow. The gravitational effects are easily estimated if the density of the slurry is known; but the friction losses are more difficult to estimate. Two types of friction mechanisms are known to be important in slurry pipeline flow [Shook et al. (2002)]:

1. Kinematic friction which increases approximately with the square of the mixture velocity,
2. A velocity independent type of friction that occurs when particles that are not completely suspended by turbulence come into contact with the pipe wall. This form of friction is referred to as contact load friction, sliding friction, or Coulombic friction.

A major advancement in the understanding of the Coulombic friction contribution to pipeline pressure losses was made at Queen's [Wilson (1976)]. Further developments have been made over the years by the Saskatoon based group [Shook et al. (1986); Gillies et al. (1991); Gillies & Shook (1994); Gillies et al. (2000); Gillies & Shook (2000); Schaan et al. (2000); Schaan & Shook (2000); Shook et al. (2002); Gillies et al. (2004); Sanders et al. (2004).]

The contribution of the particles to kinematic friction has not received as much attention. Experiments carried out by the Saskatoon group [Schaan (2001) & Gillies et al. (2004)] have shown that slurry kinematic friction is complex and that it requires more study.

The research objectives of this study are:

1. To expand the database available for assessing slurry kinematic friction by carrying out pipe flow experiments using:
 - a. Particles finer than 90 μm .
 - b. Particles that have a density different from sand.
2. To develop an improved correlating method for predicting the particle contribution to kinematic friction for slurry pipeline flows.
3. To develop a laboratory method for estimating the limiting particle concentration beyond which the frictional resistance to pipeline flow will be infinitely high.

The underlying concepts mentioned here, such as the kinematic friction component and the limiting particle concentration, are described in greater detail in the following chapter (Chapter 2 – Theory). The experimental methods and equipment used in this research are described in Chapter 3 and the experimental results and analysis are presented in Chapter 4. The conclusions and recommendations for future work are presented in Chapter 5.

2 THEORY

The mechanical energy balance for a section of slurry pipeline with a constant diameter operated under steady state conditions and carrying an incompressible fluid can be written as

$$\frac{dP}{dz} + \rho g \frac{dh}{dz} + \frac{4\tau_w}{D} = 0 \quad (2.1)$$

The three terms of the above equation represent the pressure, gravitational, and frictional contributions to the mechanical energy balance.

In laboratory research studies, the pipe is often oriented horizontally so that the gravity term is eliminated. In that case, the measured pressure gradient over a section of pipe provides a direct measurement of the friction loss when the pipeline is operated at constant flow rate.

For Newtonian fluids, the friction factor can be estimated with good accuracy from the pipeline Reynolds number and from the pipe wall roughness using a correlation such as that of Churchill (1977). If the Fanning friction factor (f) is used, then the average shear stress at the pipe wall is linked to the pipe bulk velocity (V) through

$$\tau_w = 0.5f\rho V^2 \quad (2.2)$$

To simplify the analysis of the friction losses associated with pipeline flow of slurries, it is useful to divide the slurry into three components [Shook et al. (2002)]:

1. The carrier fluid which consists of the liquid and very finely divided solids such as clays
2. The fraction of the particles that are suspended through the mixing effects due to turbulence
3. The fraction of the particles that are supported through contact with the pipe wall.

The suspended particles will contribute to velocity dependent kinematic friction while the supported particles will contribute to velocity insensitive Coulombic friction.

The frictional contributions of particles supported through contact with the pipe wall have been dealt with by Durand & Condolios (1952), Wilson (1976), and many others including Gillies (1993) and Shook et al. (2002).

The work conducted here is concerned with the frictional contributions of the carrier fluid and the particles suspended by the mixing effects of turbulence. The experiments carried out in this study were carefully chosen to minimize Coulombic friction so that the results could be directly applied to improving the understanding of the contribution of the suspended solids.

Two very different methods have been used in the past to quantify the frictional contributions of the suspended particles. Wasp et al. (1970) used a slurry viscosity

approach and other researchers have used an approach commonly referred to as the pseudofluid approximation. In the Wasp approach, the contribution of the carrier fluid and suspended solids to the overall wall shear stress is estimated as follows:

$$\tau_w = 0.5f_m\rho_mV^2 \quad (2.3)$$

In the above equation, ρ_m is the density of the mixture consisting of the carrier fluid and the suspended solids; and f_m is the Fanning friction factor for the mixture. Using Wasp's slurry viscosity approach, this Fanning friction factor, f_m , would be determined using a Reynolds number determined from the slurry viscosity μ_m as follows:

$$\text{Re}_m = \frac{DV\rho_m}{\mu_m} \quad (2.4)$$

The pseudofluid approximation assumes the frictional contribution of the vehicle is proportional to the density of the vehicle. Using this method, the contribution of the carrier fluid and suspended solids is estimated to be:

$$\tau_w = 0.5V^2\rho_m f_f \quad (2.5)$$

The Fanning friction factor is determined from the Reynolds number for the carrier fluid:

$$\text{Re}_f = \frac{DV\rho_f}{\mu_f} \quad (2.6)$$

Spells (1955) recognized the inadequacy of the pseudofluid approximation and attempted to define its limits of applicability.

Recognizing the limits of the slurry viscosity approach and the pseudofluid approximation, others have attempted to develop better methods to estimate the frictional contributions of suspended particles. The most useful of these methods are described in this chapter.

If the slurry viscosity approach is used, the effect of particle concentration on mixture viscosity must be measured or estimated. In practice, measurements are rarely made and thus the slurry viscosity approach relies almost exclusively on the use of correlations. Many correlations are available to estimate the viscosity of a mixture μ_m including the following one which was proposed by Thomas (1965):

$$\frac{\mu_m}{\mu_f} = 1 + 2.5C + 10.05C^2 + 0.00273e^{16.6C} \quad (2.7)$$

In the above correlation, μ_f is the viscosity of the carrier liquid and C is the volume fraction of the mixture which is occupied by particles, i.e. the solids volume fraction.

Slurry pipeline studies carried out by Schaan (2001) and by Gillies et al. (2004) used relatively fine sand as the solids component so that Coulombic friction could be neglected and the measured pressure losses could be used to provide direct estimates of kinematic friction. A relatively fine and narrowly graded sand with an average particle diameter of 92 μm was used and the tests were carried out in

pipelines with nominal diameters of 50, 100, and 150 mm. These studies provide insight into the limitations of the two common methods for estimating slurry pipeline kinematic friction. In Figure 2.1 the 92 μm sand slurry data are used to examine the suitability of the slurry viscosity approach. Equation (2.7) was used to estimate the slurry viscosity. The friction factors were determined using Equations (2.1) and (2.3) assuming that the pipe wall was hydraulically smooth. The researchers reported very low pipe wall roughness values with relative roughness values less than 0.0001. It is apparent that the slurry viscosity based f - Re relationship does not provide good estimates of the slurry friction factor for the 92 μm sand slurries. If the slurry viscosity method was valid, the experimental data points would have fallen on the line representing the friction factor-Reynolds number relationship for Newtonian fluids. The significant variation with pipe size is especially troubling in that the method cannot be expected to provide good scale up estimates for the design of large diameter industrial pipelines.

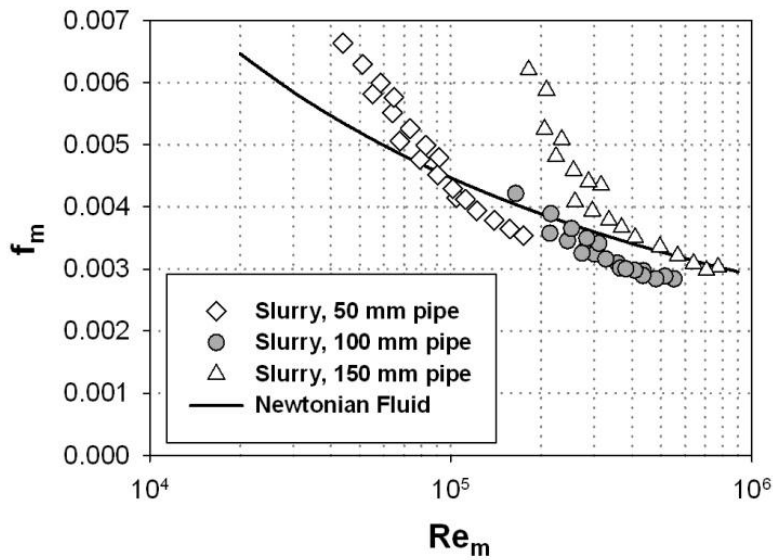


Figure 2.1 A comparison of experimentally determined friction factors for 92 μm sand-in-water slurries with expected friction factors obtained using the slurry viscosity method.

Figure 2.2 shows that the pseudofluid approximation (Equation 2.5) may be useful for relatively low sand concentrations ($C = 0.15$) with the experimental data points falling near the water friction curve. However, the method significantly underestimates the friction losses for more concentrated slurries ($C = 0.29$ and 0.38).

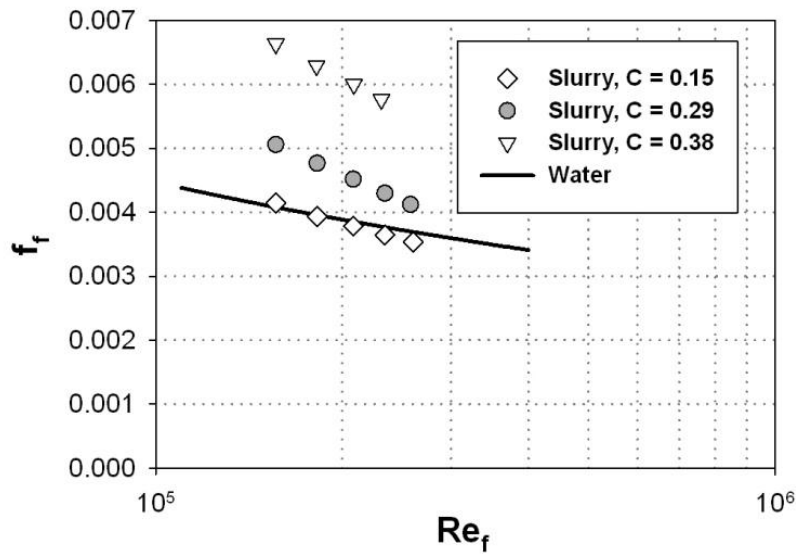


Figure 2.2 A comparison of experimentally determined friction factors for 92 μm sand-in-water slurries flowing in a 50 mm pipe with expected friction factors obtained using the pseudo-fluid slurry approximation.

The limitations of the slurry viscosity approach and the pseudofluid approximation, which both essentially treat the mixture as if it were a fluid, have been known for more than 50 years. In the subsequent section, the notion that the wall shear stress for the mixture is a sum of two components (one due to the fluid and one due to the particles) is introduced and discussed. Also in this section, the importance of the limiting (maximum) volume fraction, C_∞ , in slurry flow calculations is described. The parameter C_∞ , the concentration at which the distance between adjacent particles approaches zero and the slurry's resistance to flow approaches an infinite value, is very important to the understanding of friction losses of pipeline slurry flows.

Bagnold (1954) interpreted the torque measurements from a Couette device by assuming that the wall stress τ_w was the sum of fluid and particle stresses:

$$\tau_w = \tau_f + \tau_s \quad (2.8)$$

Bagnold found that the particle stress was strongly dependent on λ , the linear concentration of the particles. He also found that the particle stress was independent of particle diameter for relatively fine particles and that the particle stress increased with the square of particle diameter for relatively coarse particles. The linear concentration is calculated using the volume concentration of particles, C and C_∞ :

$$\lambda = \left[\left(\frac{C_\infty}{C} \right)^{1/3} - 1 \right]^{-1} \quad (2.9)$$

An important aspect of C_∞ is that it can be used for predicting the deposition velocity, V_c , for pipeline flow of intermediate-sized particles. Sanders et al. (2004) found that the deposition velocity can be predicted using the following equation for dimensionless deposition velocity, V_c^*

$$V_c^* = \frac{V_c \sqrt{f/2}}{[g\mu_f (S_s - 1)/\rho_f]} = \frac{0.76 + 0.15d^+}{[(C_\infty - C)^{0.88}]^{1/3}} \quad (2.10)$$

The parameter C_∞ can be estimated in a number of ways. A simple method for determining C_∞ is to perform settling tests. A known mass of particles of known solids density is added in slurry form to a graduated cylinder. The particles are allowed to freely settle and are also manually tamped to promote maximum settling. The ratio of the volume of particles added to the cylinder to the volume

occupied by the packed bed of particles gives the maximum packing concentration, C_{∞} .

Singh et al. (2001) conducted settling tests with mixtures of multisized particles. It was found that an increase in the height of the settled bed causes an increase in the settled concentration, or C_{∞} . Also, it was found that the initial concentration of the sample has a small effect on the predicted value of C_{∞} . Singh presented an example where the maximum particle concentration was measured at a number of initial concentrations, ranging from 11% to 26% by volume, and the maximum particle concentration varied by less than 2%.

Hoffmann & Finkers (1995) presented a semi-empirical correlation to determine the void fraction in randomly packed particle beds given particle properties. The void fraction, ε , is the concentration of voids in a packed bed:

$$\varepsilon = 1 - C_{\infty} \quad (2.11)$$

Hoffmann & Finkers used a theoretical basis to determine the general form of the correlation and then used data from many sources to fit the constants of the correlation. Correlations are available for both loosely packed and tapped beds. For the purposes of this study, the definition of the loosely packed beds most accurately describes the system. Hoffmann and Finkers' void fraction correlation for loosely packed beds is:

$$\varepsilon = 1 - \left\{ 1 - \left[(1 - 0.416)e^{-0.0142\rho'd_{s0}} + 0.416 \right] e^{-0.829\sigma} \right\} \phi^{0.862} \quad (2.12)$$

where ρ' is the dimensionless density, given by the particle density divided by the density of water; d_{50} is the mean particle diameter in units of μm ; σ is the standard deviation of the particle size distribution; and φ is the sphericity of a particle. The correlation is expected to apply when: $\rho'd_{50} < 20$, $\sigma > 0.69$, and $\varphi > 0.15$. The particle density and average diameter have no effect on the calculated values of the infinite concentration for the particles studied here. As Hoffmann & Finkers state, these parameters only affect the expression when the particles are very small (sub-micron) or very light. For the particles in this study, the parameters that govern the expression are the standard deviation of the size distribution and the particle sphericity. The effect of the size distribution is easy to understand. With a broader size distribution, a lower void fraction would be expected since smaller particles would be able to fill in the voids between the larger particles. As the particle shape becomes less spherical the voidage increases or the infinite concentration decreases.

C_∞ can also be determined from experimental data from pipe loop tests and viscometer tests [Schaan (2001)]. These methods are presented in greater detail in Chapter 4.

It is evident that accurate measurements of C_∞ will be required to develop accurate expressions for the particle contribution to the kinematic friction. The various methods available for determining C_∞ are compared within this study.

Now that Bagnold's (1954) approach to separating the solids and fluid contribution to wall shear stress has been introduced, and the importance of the

limiting concentration C_∞ has been described, it is possible to present the most recent work done to predict the frictional contributions of suspended particles. In this regard, an important study was conducted by Shook & Bartosik (1991). Using a vertical pipe to eliminate any Coulombic contributions to friction losses, Shook & Bartosik used an excess friction loss term to assess kinematic friction for particle-liquid systems. The excess friction loss depends on the measured friction loss for the mixture, the friction loss for the carrier fluid flowing by itself, and the concentration of the particles as follows

$$\phi = \frac{\tau_w - \tau_{w,f}}{\tau_{w,f} C} \quad (2.13)$$

Shook & Bartosik concluded that their wall stresses appeared to be related to those discovered by Bagnold. They found that the excess friction loss decreased with increasing pipeline velocity and with increasing particle size. They also found that for relatively fine particles, the excess friction loss increased with increasing particle concentration.

Some years later, Shook revisited the problem [Shook et al. (2002); Shook et al. (2004)] and adopted Bagnold's approach of using separate fluid and particle stress contributions in an effort to obtain improved estimates of the kinematic contribution of the particles. Shook and his coworkers assumed that the kinematic contribution to wall shear stress could be written as follows

$$\tau_k = \tau_{w,f} + \tau_{k,s} = 0.5 f_f \rho_f V^2 + 0.5 f_s \rho_s V^2 \quad (2.14)$$

The above equation is useful only if f_s , the solids friction factor, can be estimated with a satisfactory degree of accuracy. Shook et al. (2004) tentatively proposed the following correlation

$$f_s = \lambda^{1.25} \left[0.00005 + 0.00033e^{-0.1d^+} \right] \quad (2.15)$$

In the above correlation, d^+ is the dimensionless particle diameter, which is

$$d^+ = \frac{du_* \rho_f}{\mu_f} = \frac{d(f_f/2)^{0.5} V \rho_f}{\mu_f} \quad (2.16)$$

While Shook and co-workers did not state this explicitly, it seems likely that their kinematic friction correlation was intended to represent a balance between the particle stress effect recognized by Bagnold and lift effects that are known to act on particles located near the pipe wall.

Saffman (1965) determined that a particle in a sheared fluid experiences a force acting perpendicular to the direction of shear. He found this lift force could be described using the following expression:

$$F_{lift} = 1.6\mu dv_\infty \left(\frac{\rho_f d^2}{\mu} \dot{\gamma} \right)^{1/2} \quad (2.17)$$

While the above equation was developed for Poiseuille flow (i.e. laminar flow in a tube), the concept should also apply to turbulent pipe flow if the analysis is limited to the region very near the wall where viscous effects dominate.

In the near-wall region, the dimensionless velocity (v/u^*) is equal to the dimensionless distance from the wall ($d u^* \rho/\mu$). Therefore, the change in velocity with respect to distance from the pipe wall is

$$\dot{\gamma} = \frac{\rho u_*^2}{\mu} \quad (2.18)$$

By combining Equations (2.17) and (2.18), the following expression is obtained for the lift force acting on a particle in the vicinity of the pipe wall

$$F_{lift} = 1.6 \mu d v_\infty d^+ \quad (2.19)$$

From Equation (2.19) we see that, as the dimensionless particle diameter increases, the lift force acting on a particle in the near wall region of the pipe should also increase thus counteracting the effects of the Bagnold stress on the particle contribution to kinematic friction. This finding is qualitatively consistent with the Shook correlation (Equation 2.14) as demonstrated in Figure 2.3.

A considerable body of work has been published by K.C. Wilson and co-workers including recent studies by Wilson and Sellgren (2008) and Wilson et al. (2010) to examine near-wall particle lift effects in slurry pipelines. While the work does provide useful insight into the nature of the near-wall lift phenomenon, unfortunately no attempt was made to separate the kinematic contribution of the particles from Coulombic friction. The Shook approach avoids the uncertainties associated with Coulombic friction and appears to provide a more useful starting point for this study.

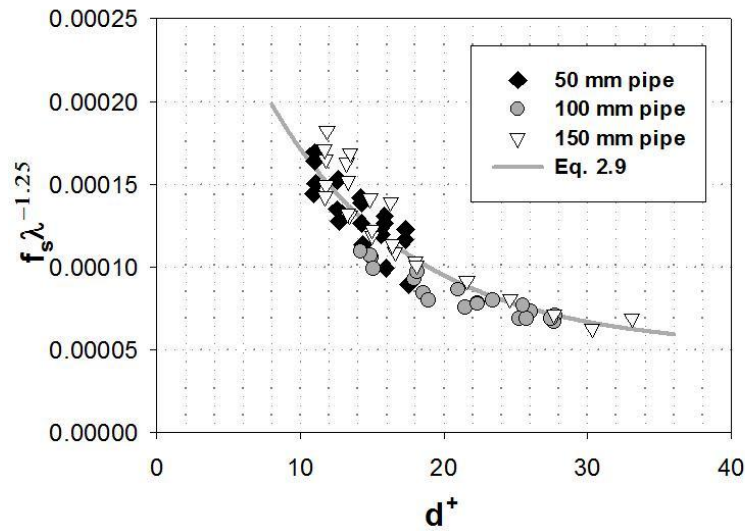


Figure 2.3 A comparison of the predictions of the Shook correlation and experimental data for pipeline flow of 92 μm sand-in-water slurries.

Figure 2.3 shows that Equation (2.15) provides quantitatively reasonable predictions of the particle friction factor for 92 μm sand-in-water slurries. Equation (2.15) is found in the SRC's slurry flow model [Gillies et al. (2004)] which is used extensively in the design and operation of the very large pipelines used to transport ore and tailings mixtures in Alberta's oil sands operations. While the correlation is undoubtedly useful, it was developed from a very limited database consisting mainly of experimental data for sand-in-water slurries.

The work of Shook et al. (2002) shows the slurry viscosity method and the pseudofluid approximation are too simplistic to deal with the complexities of slurry flows. Neither of the older methods takes the very important effect of particle diameter into account when estimating the frictional contribution of the suspended particles.

The objective of this study is to expand the database to include a broader range of fluid viscosities, particle sizes, and particle densities. Previously unpublished data provided by the SRC and new data generated in the experimental component of this study are to be used to validate Equation (2.14) and to provide an improved correlation method for estimating kinematic friction for the pipeline flow of slurries.

3 EQUIPMENT, MATERIALS & PROCEDURES

3.1 Pipeline Loop

A 75 mm inner diameter steel pipeline was used for the bulk of the tests. A schematic of the pipeline is presented in Figure 3.1.

The pipeline length was 43 m and the loop had a volume of 202 L. A cylindrical tank (330 L volume) with a conical bottom was located before the pump inlet. The 180° change of direction at the midpoint of the pipeline loop was achieved by using a pipe section bent to a 0.6 m radius. In comparison with standard elbows, it is expected that this bend will reduce flow disturbance.

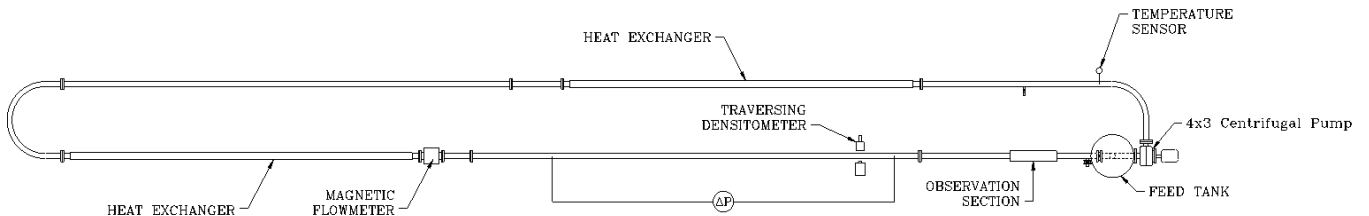


Figure 3.1 75 mm pipeline loop and instrumentation

A Warman 4/3 AH centrifugal slurry pump was used to circulate the slurries. The pump was powered by a 40HP (30 kW) electric motor. The mixture velocity was adjusted by changing the motor speed. This was accomplished through the use of a Benschaw Advanced Controls & Drives variable frequency controller.

A temperature sensor was located in the line after the pump outlet. The temperature sensor was calibrated in a water bath using a thermometer with a

precision of 0.1°C. Two counter-flow pipe-over-pipe heat exchangers were located on the pipeline covering an area of 3.4 m². A 50/50 Ethylene glycol/water mixture was pumped through the annulus of the pipes to control the temperature.

A 2800 series Foxboro magnetic flow meter was used to determine the volumetric flow rate of the slurry. The magnetic flow meter was calibrated with water using a bucket and stopwatch method.

A 6 m long test section was located 10 m from the pipe bend on the pump inlet side to ensure fully developed flow through the section. The pressure drop across the test section was measured with a Validyne model DP-15 differential pressure transducer. The pressure transducer was calibrated using a U-tube Manometer filled with Meriam fluid (density = 2950 kg/m³). The internal diameter of the test section had been determined by SRC to be 75.39 mm. This determination was made by measuring the volume of water required to fill the section of known length. Pressure tapings (3.2 mm in diameter) were used with the upstream tapping located 100 pipe diameters downstream of the nearest flow disturbance. The pressure taps were located at 45° above the center of the pipe, a “compromise” position that minimizes plugging of the pressure sensing line by particles while reducing the likelihood of stray air bubbles entering the sensing line.

A traversing gamma ray densitometer was installed near the end of the test section and was used to measure the solids concentration distribution in the pipe and the total solids concentration in the slurry. By monitoring the solids concentration

near the bottom of the pipe over a range of pipeline operating velocities, it was also possible to determine the critical velocity corresponding with the onset of particle deposition. This densitometer is described in detail in Section 3.2.1.

A section of acrylic pipe was located before the pump inlet which allowed the deposition velocity to be visually determined.

All signals from these instruments were sent as dc voltages to an InstruNet model 100 Analog/Digital Input/Output System and were converted to digital outputs to be used within SRC's data acquisition software. This software required calibration information to convert the outputs to engineering units for each instrument.

3.2 Pipeline Test Procedure

The SRC data acquisition software allowed constant monitoring of pipeline operating temperature, velocity, pump RPM, test section ΔP , and gamma ray densitometer count rates.

Before each slurry run, the pipeline was filled with water and the water was partially de-aerated. To remove air, the water in the pipeline was heated up to 45°C to reduce its dissolved air content. The water was then circulated at a sufficiently low velocity so that air bubbles would travel along the top of the pipe and could escape into the inlet tank. Once the water had been de-aerated, a pressure loss run was performed. With the pipeline operating temperature held constant, the pressure loss was recorded as a function of velocity over a range of velocities from the highest achievable velocity of the pump down to no flow.

This allowed determination of the pipe wall equivalent roughness, an important parameter for the tests.

Solids were then added to the pipeline. The pipeline was operated at a speed of approximately 3 m/s and solids were slowly poured into the tank. A recycle valve connecting the pump outlet portion of the pipeline to the bottom of the tank was opened to allow the solids to be washed from the tank into the pipeline. Once the desired mass of solids had been added, the pipeline was heated to 45°C and the de-aeration procedure was repeated.

For each slurry run, the temperature was set and controlled at either 20°C or 40°C. Two types of tests were performed on each slurry: pressure loss runs, and traversing gamma ray scans. For each data point reported here, data were collected for 60 seconds, once sufficient time had been allowed for the system to reach equilibrium at the desired conditions. The software was programmed to collect data at 1 ms intervals and the average over the 60 second period was reported and stored in a data file.

For pressure loss runs, a data point was collected at the highest achievable velocity (approximately 7 m/s). Successive data points were then collected by reducing the velocity in increments of ~1 m/s. At lower velocities, particles were observed in the acrylic pipe section sliding along the bottom of the pipe, which was an indication that the system was nearing the deposition velocity. At this time, much smaller intervals were used and a few data points were taken after deposition was visually observed in the acrylic section. Before and after each run,

“zero readings” were taken. These readings were data points taken with no flow in the pipeline to allow any offsets of instruments to be measured. The pressure loss runs were conducted with the gamma ray densitometer set at $y/D = 0.05$ (see Fig 3.2) for each data point.

After the pressure loss run, a traversing gamma scan of the pipe was performed. The purpose of the gamma scan was to measure the exact concentration in the pipeline. In this scan, the velocity of the slurry was set high enough to ensure uniformly dispersed flow (typically around 3 m/s) and gamma ray scans were taken at different vertical positions ranging from $y/D = 0.95$ to $y/D = 0.05$ in 0.10 increments. An air scan was performed before and after each traversing gamma scan. The data collected during the air scan were subtracted from the slurry data to reduce background noise.

The gamma ray densitometer used is shown in Figure 3.2. The Cesium-137 source and casing produced the collimated gamma ray radiation to be sent across the pipe. A collimated beam, 2 mm in height, was produced by cutting a slit in a lead block. The radiation intensity was measured with a detector on the other side of the pipe. The beam would enter the detector through another narrow slit of 2 mm and the counts of radiation would be measured and the output sent to a computer.

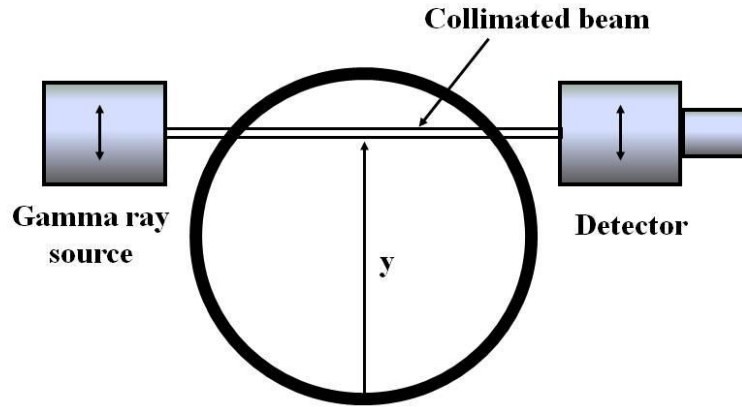


Figure 3.2 Gamma ray densitometer; pipe diameter is D .

Before using the densitometer in experiments, the absorption coefficients of the steel pipe, water, and each of the solids tested during this project were determined. Also, the path length at each y/D value needed to be measured.

Using the Beer-Lambert law (as reported by Shook & Roco (1991)) the absorption coefficient for the various mediums used in the experiments can be found:

$$\ln\left(\frac{N}{N_0}\right) = -\sum a_j x_j = -a_w x_w - a_f x_f - a_s x_s \quad (3.1)$$

where N_0 is the intensity observed in a medium of air or the unattenuated beam intensity, N is the intensity observed through the medium in question, a_j is the absorption coefficient, and x_j is the path length. The subscript w denotes pipe wall, f denotes liquid or water, and s denotes solids.

To determine the absorption coefficient of the steel pipe wall the degree of attenuation of a beam travelling through a mild steel plate of known thickness was measured. The absorption coefficient for water was determined by measuring the degree of attenuation in a water-filled cylinder where the path length was known. The absorption coefficients for each of the particle types were similarly determined by measuring the degree of attenuation along a known path length through a cylinder filled with a packed bed of particles and water.

The path length of the pipe wall was found, once the absorption coefficient of the pipe was determined, by measuring the intensity of the beam (N) travelling through the empty pipe at ten discrete positions from $y/D = 0.05$ to $y/D = 0.95$. The path length was calculated using Eq. (3.1), with the last term on the RHS set to 0. For the actual experiments, when slurry was in the pipe, the determination of the concentration was estimated from

$$\ln\left(\frac{N}{N_0}\right) = -a_w x_w - a_m x_m \quad (3.2)$$

where x_m is the same path length as for water alone, and a_m is measured. The local concentration for each vertical chord is then given by:

$$c = \frac{a_m - a_f}{a_s - a_f} \quad (3.3)$$

Since the path length at each vertical position is different, an average pipeline concentration must be determined using the chord-averaged concentrations. This

average concentration can be calculated by integrating the local concentration numerically over the cross-section of the pipe:

$$C = \frac{\sum_{j=1}^n c_j L_j}{\sum_{j=1}^n L_j} \quad (3.4)$$

where C is the average concentration, c_j is the chord-averaged concentration, and L_j is the chord length [Gillies (1993)].

3.3 Laboratory Tests

3.3.1 Concentric Cylinder Viscometer Tests to Determine C_∞

Apparatus

A HAAKE Viscotester 550 (VT550) was used for the experiments conducted to determine the limiting concentration, C_∞ . The VT550 is a concentric cylinder viscometer in which a spindle rotates at a preset speed, ω , in a cup of fluid and the torque, T , required to rotate the spindle is measured. The spindle used for this study had a radius, R_1 , of 18.4 mm and a length, L , of 60 mm. The cup had a radius, R_2 , of 21 mm. A schematic of the concentric cylinder viscometer is presented as Figure 3.3. The HAAKE RheoWin software was used to record the spindle speed and the resulting torque and control programs were created to ramp up or down the speed for a set of measurements. Glycol was pumped from a temperature controlled bath to the viscometer apparatus to heat or cool the fluid. The bath temperature was controlled by the HAAKE RheoWin software.

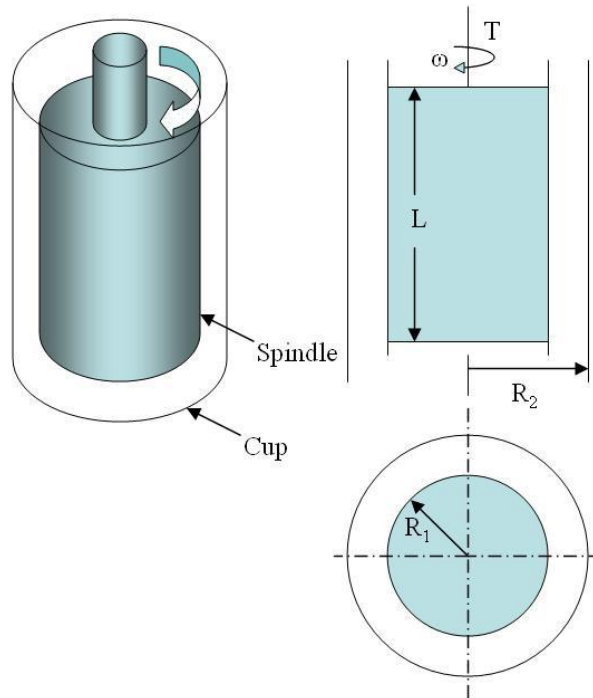


Figure 3.3 Concentric Cylinder Viscometer

Procedure

Slurries of different types of particles suspended in a glycol-glycerol mixture were tested at different concentrations. The glycol-glycerol mixture was approximately 75% glycerol and 25% glycol by volume. The mixture had a viscosity of 300 mPa·s at 22°C.

The following procedure was used for each concentration and particle type. A sample of the glycol-glycerol mixture was placed in a beaker. The temperature of the sample was measured (typically 22°C to 24°C) and the sample temperature was entered in the HAAKE RheoWin program. Once the bath temperature reached that of the sample, a run was performed.

Each run involved the collection of eight data points, ramping up from the lowest speed to the highest in four steps and then back down again. This procedure was used to verify Newtonian fluid behaviour. After testing the carrier fluid it was placed back into a beaker and the correct mass of particles was added. The contents were mixed by hand to ensure a homogenous slurry and to release any entrained air. The speed of mixing in the beaker was purposefully kept sufficiently low to avoid viscous heating of the slurry. The temperature was then measured again and had to be within 0.5°C of the original carrier fluid test or else the test was restarted. The slurry was then tested in the viscometer using the same procedure as that used to determine the viscosity of the carrier fluid. During a limited number of runs, a mixture would appear to exhibit shear thinning behavior as the measured torque was lower during the “step-decrease” cycle than they were at identical spindle speeds during 1st half of the cycle. This result was attributed to particle settling within the cup. When this occurred, the data points affected by settling were rejected.

3.3.2 Particle density determination

Apparatus

The density of the different particles was measured using four 200 mL volumetric flasks. These flasks were then vacuum aspirated to remove entrained air in the slurries.

Procedure

The four flasks were weighed empty and then approximately 50 mL distilled water was added to each flask. A similar volume of particles was added and the flasks were capped and gently shaken until the contents were well mixed. The total volume was then adjusted by adding distilled water so that the meniscus was at the 200 mL mark of the flask.

The flasks were then connected to the aspirator to de-aerate the slurries. The suction was carefully monitored to ensure no slurry escaped. After aspirating the samples, more water was added (if needed) to ensure the total volume was 200 mL. The mass of the flask was then taken, since the mass of the empty flask was known, the mass of the slurry could be determined. The slurry was then carefully washed into a pre-weighed dish. The dish was dried in an oven at 100°C for 24 hours and the total mass of solids in the slurry was determined. After cleaning out the flasks, they were re-filled with distilled water and using the density of water, the volumes of the flasks were determined. The density of the particles could then be calculated from the volume of the flasks, the mass of the solids and the mass of the slurry.

3.3.3 Particle Size Determination

The mass median diameter of the particles, d_{50} , was determined using the dry sieving technique (particles $> 44 \mu\text{m}$ in size) and an Andreasen Pipette (particles $< 44 \mu\text{m}$ in size).

Sieving Apparatus

For dry sieving, a series of six sieves was used. The smallest sieve, which had 45 μm openings, was placed over a pan. The remaining five sieves were placed in order of increasing opening size above the 44 μm sieve.

Procedure for sieving

A mass of particles was placed on the top screen and then the sieves were placed in a shaker for 30 minutes. Each sieve was then weighed to determine the mass of solids collected on each sieve. The $< 44 \mu\text{m}$ particles were collected and then analysed with an Andreasen Pipette.

Andreasen Pipette

An Andreasen Pipette is an instrument used to determine the particle size distribution of fine ($< 44 \mu\text{m}$) particles. The instrument consists of a graduated cylinder with a modified top. The pipette portion is completely made of glass, including a glass pipette tube that sits a few centimetres from the bottom of the cylinder. This tube attaches to the 10 mL volume pipette bulb. A three-way valve allows fluid to either travel into the pipette bulb from the cylinder or be expelled from the bulb into a dish. A photograph of the pipette used is presented as Figure 3.4.



Figure 3.4 Andreasen pipette

Andreasen Pipette Procedure

A slurry of approximately 1% solids by volume was prepared in the graduated cylinder of the instrument. The contents were well mixed and the cylinder was placed on the bench top. Immediately a timer was started. At certain time intervals (e.g. 30 seconds, 60 seconds, 120 seconds) a 10 mL sample of fluid was suctioned from the cylinder and placed in a dish to dry. Great care was taken during this suction process to not disturb the suspension settling in the cylinder.

The Stokes settling velocity equation was used to determine the diameter of the particles taken at each time interval. For a single spherical particle settling in a Newtonian fluid, the settling velocity is found by:

$$v_{\infty} = \left[\frac{4gd(\rho_s - \rho_f)}{3C_D\rho_f} \right]^{1/2} \quad (3.5)$$

For spherical particles fine enough to settle in the Stokes region ($Re_p < 0.3$), the drag coefficient is:

$$C_D = \frac{24}{Re_p} \quad (3.6)$$

where

$$Re_p = \frac{dv_{\infty}\rho_f}{\mu_f} \quad (3.7)$$

The particle diameter can thus be estimated for very dilute concentrations of spherical particles settling in the Stokes region:

$$d = \sqrt{\frac{18v_{\infty}\mu_f}{g(\rho_s - \rho_f)}} \quad (3.8)$$

By taking samples at known time intervals from the same position in the cylinder, determining the weight percentage of solids in each sample, and calculating the particle diameter of each sample using the Stokes equation, a particle size distribution of the < 44 μm could be created.

The analysis presented above is based upon the assumption that Stokes Law is valid and that the particles are spherical. Although the particles studied here were not spherical, this assumption should not introduce an error since at low Reynolds numbers spheres and disks (which are vastly different in shape) have very similar drag coefficients. This can be seen in any drag coefficient vs. particle Reynolds number curve such as the one presented by Perry (1963).

3.3.4 Settling Tests to Determine C_{∞}

Procedure

A known mass of particles was placed in a 1000 mL graduated cylinder. Distilled water was then added to make a solids concentration of 30% by volume. The cylinder was plugged using a rubber stopper and then the slurry was thoroughly mixed. The cylinder was left undisturbed until all particles had settled and the liquid above the bed was completely clear (this could take anywhere from 24 hours to 5 days depending on the particle type). Once settling was complete, the volume occupied by the settled bed of particles was recorded and manual tamping (lifting up the cylinder and tapping the bottom gently on the countertop) was performed to promote the formation of the settled bed. The settling process was repeated until the volume of the settled bed did not change.

Once the volume of particles in the packed bed was known, the cylinder was filled to that volume with distilled water and the mass of water was recorded to determine the true volume of the cylinder. The volume of particles added to the

cylinder was known and by measuring the volume occupied by particles, the maximum packing concentration could be determined.

4 RESULTS AND DISCUSSION

4.1 Particle Characterization

Four particle types were used in the experiments: aluminium oxide, an angular sand (Lane Mountain 125), silica flour (Sil 325), and petroleum coke supplied by Syncrude Canada Ltd. The particles were chosen such that effects of particle density, size, and shape on kinematic friction (and C_{∞}) could be studied. Photographs of each particle type along with a scale are presented in Figures 4.1 through 4.4.

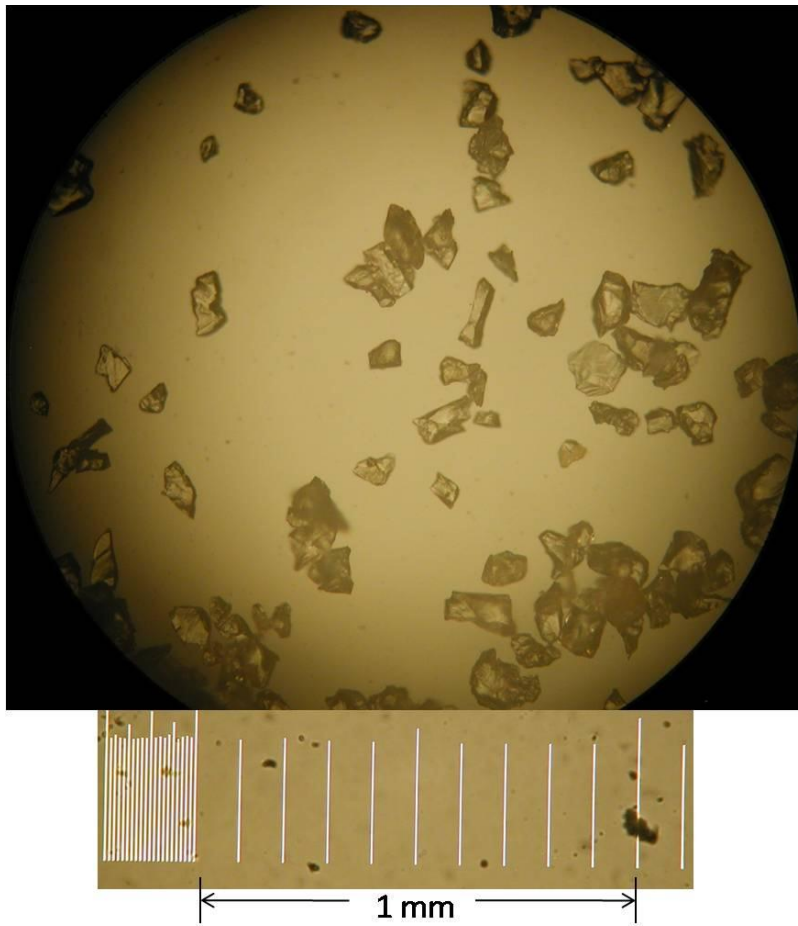


Figure 4.1 Photograph of aluminum oxide particles

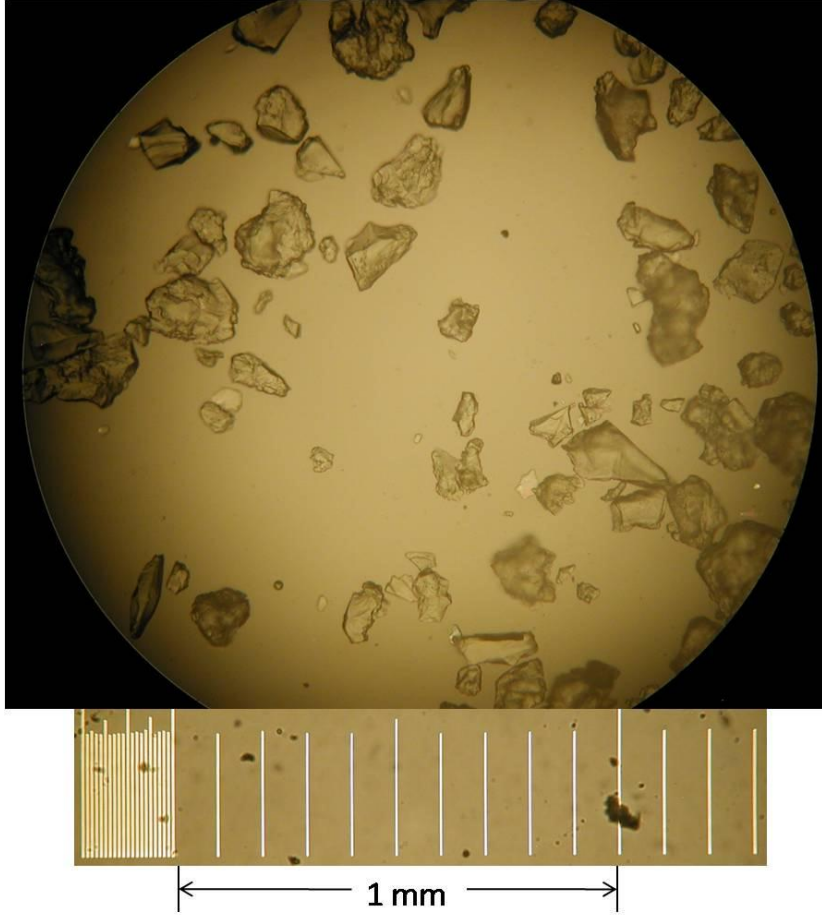


Figure 4.2 Photograph of angular sand particles (Lane Mountain 125)

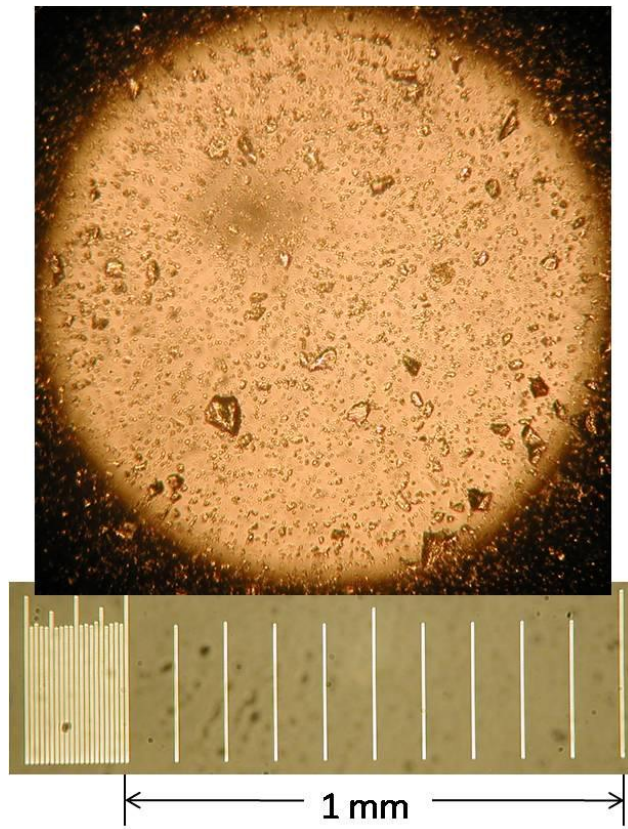


Figure 4.3 Photograph of silica flour particles (SIL 325)

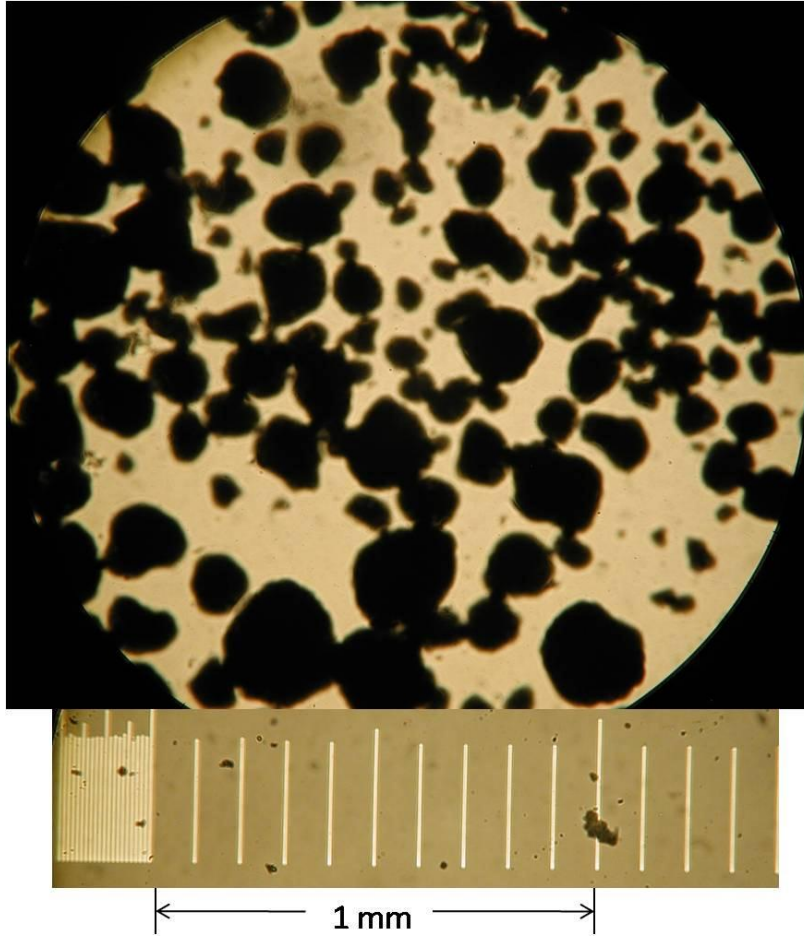


Figure 4.4 Photograph of petroleum coke particles

Dry sieving was used to determine the particle size distribution of each of the four particle types. Both the petroleum coke particles and the angular sand particles had less than 3% fines by weight, smaller than 44 μm in diameter. For the aluminium oxide particles, it was found that 10% of the particles were fines and for the fine silica flour all particles were less than 44 μm in diameter. It was necessary to determine the size distribution of the particles less than 44 μm in diameter. To do this, an Andreasen Pipette was used.

The particle size distributions are plotted in Figure 4.5 and can be found in tabular form in Appendix A.

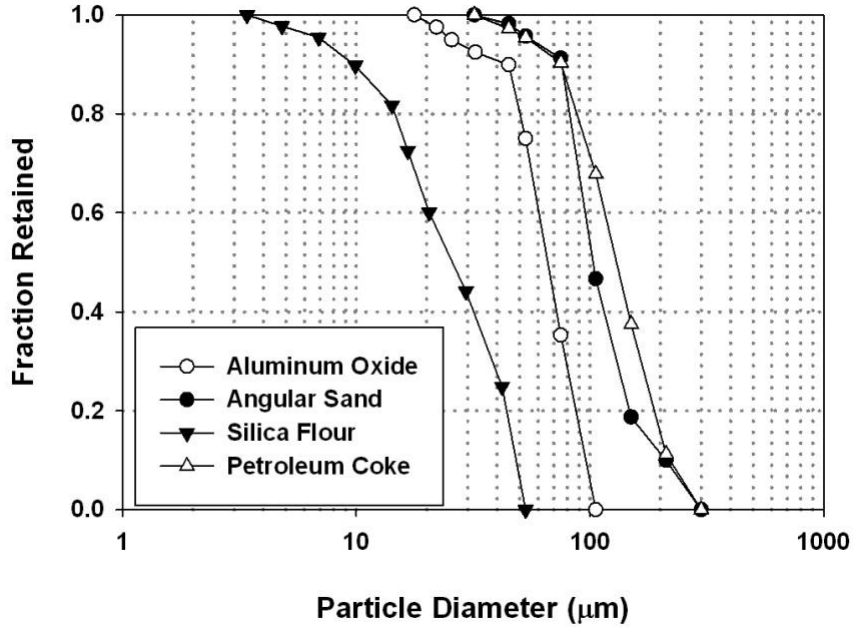


Figure 4.5 Particle size distributions

The d_{50} , or mass median diameter of each particle type, is given in Table 4.2. Particle densities, determined using the method described in Section 3.3.2, are also reported here.

The particle sphericity was determined by analyzing the micrographs. Approximately 20-30 particles of each type were photographed and the lengths of the minor and major axes of each particle were measured. The sphericity was calculated from the ratio of minor axis to major axis. This method was used to ensure consistency with existing data collected by Schaan who also used the method [Schaan et al. (2000)]. Other methods exist to calculate sphericity [Clift et al. (1978)]. The sphericity of each particle type is reported in Table 4.1. The

sphericity of the silica flour was not determined as the particles were too small to be analyzed with the microscope that was available.

Table 4.1 Properties of particles used in this study

Particles	d₅₀ (μm)	Density (kg/m^3)	Sphericity
Aluminum Oxide	67	3950	0.63
Angular Sand	104	2650	0.61
Silica Flour	28	2660	N/A
Petroleum Coke	131	1600	0.78

4.2 Pipeline Tests

4.2.1 Overview

Tests were performed in a 75 mm pipeline on slurries of aluminum oxide, silica flour, petroleum coke, and mixtures of aluminum oxide and angular sand. Pressure loss vs. velocity data were collected for each slurry type at various concentrations and temperatures of 20°C and 40°C. These data can be found in Appendix C.

Data collected from the pipeline runs for slurries prepared with aluminum oxide, angular sand, silica flour, or petroleum coke were used, along with existing data collected by other researchers at SRC [Gillies (2003); Schaan et al. (2000); Shook & Roco (1991)] to develop a new correlation for predicting the kinematic friction component in slurry pipeline flow. The other data were obtained for slurries of 92 μm angular sand in 2 inch and 6 inch diameter pipelines, and 90 μm angular sand in water and 90 μm angular sand in glycol both in a 4 inch pipeline. Each data set included the pipe diameter, equivalent pipeline roughness, velocity

vs. pressure loss, density of carrier fluid, viscosity of carrier fluid, particle diameter, particle density, and particle concentration.

The tests in this study were performed under conditions where Coulombic effects were deemed to be negligible. Only turbulent data were used in the analysis to ensure that particles were fully suspended (i.e. negligible contact load).

4.2.2 Determining C_∞

In order to determine the maximum packing concentration for each type of particles, a logarithmic fit of $\frac{f_s}{\lambda^{1.25}}$ versus d^+ was plotted, where λ was determined by varying C_∞ until the maximum regression coefficient was found. For example, Figure 4.6 shows the relationship for alumina particles. For this slurry, the value of C_∞ which had the best regression coefficient was 0.48. Note that in the figure the symbol Y represents $\frac{f_s}{\lambda^{1.25}}$ and the logarithmic trend (solid curve) has the form:

$$Y = \frac{f_s}{\lambda^{1.25}} = -0.0001 \ln(d^+) + 0.0004$$
$$R^2 = 0.9624 \quad (4.1)$$

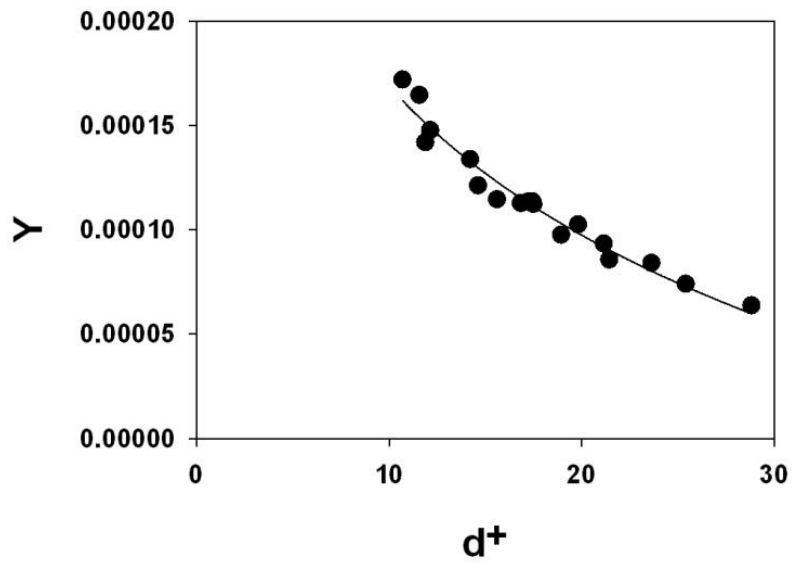


Figure 4.6 Determining C_∞ for aluminum oxide slurries from 75 mm pipeline tests using a logarithmic regression function

The values of C_∞ for each particle found from this analysis are presented in Table 4.2.

Table 4.2 C_∞ values determined from pipeline tests

Particles	C_∞ from Pipeline
Aluminum Oxide	0.48
Angular Sand	0.50*
Silica Flour	0.62
Petroleum Coke	0.57

*Schaan (2001)

4.2.3 Developing an improved correlation for f_s

Once C_∞ had been determined for each particle type by optimizing the regression coefficients, the data were plotted and then fit with two different logarithmic functions:

$$Y = \frac{f_s}{\lambda^{1.25}} = A \ln(d^+) + B \quad (4.2)$$

where for $d^+ \leq 21$:

$$\begin{aligned} A &= -1.1 \times 10^{-4} \text{ and } B = 4.2 \times 10^{-4} \\ R^2 &= 0.9742 \end{aligned} \quad (4.2a)$$

For $d^+ > 21$:

$$\begin{aligned} A &= -5.6 \times 10^{-5} \text{ and } B = 2.6 \times 10^{-4} \\ R^2 &= 0.8426 \end{aligned} \quad (4.2b)$$

These functions and the experimental data are plotted in Figure 4.7. Other fits (exponential and power) were attempted and rejected due to low R^2 values. These fits are presented in Appendix D.

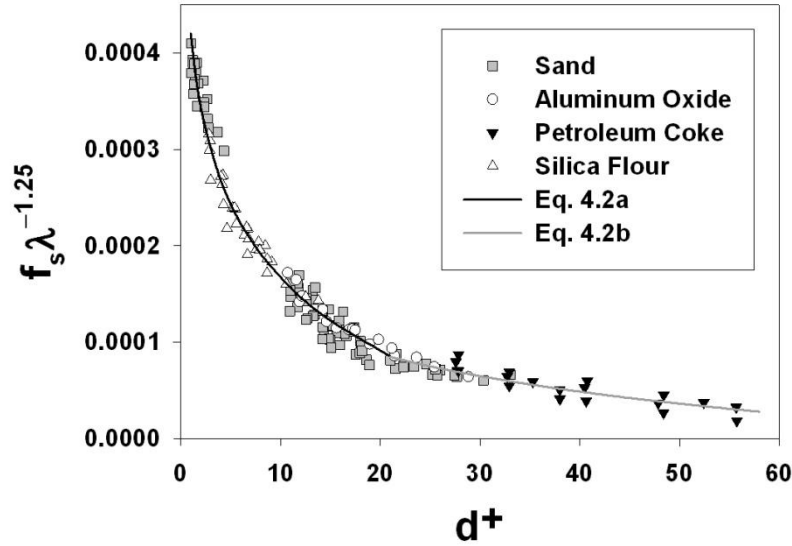


Figure 4.7 Logarithmic relationship describing kinematic friction behavior of different particle slurries

This correlation fits the experimental data well and encompasses a wide range of d^+ values. The shape of the curve also matches that described in Chapter 2. As the dimensionless particle diameter increases, the lift force acting on particles in the near wall region increases counteracting the effects of the Bagnold stress on the particle contribution to kinematic friction.

The angular sand data, which correspond to the low d^+ values, were previously collected at SRC (Gillies, 2003). Low d^+ values were obtained because the carrier fluid, glycol, had a high viscosity (4 to 10 times the viscosity of water). For every other particle type, water was used as the suspending medium. The sand data shown in the intermediate portion of the correlation ($10 \leq d^+ \leq 30$) includes both angular and rounded sand data collected by Schaan (2001).

Before the present study was completed there was no strong experimental evidence to support the use of the product $f_s \rho_s$ in Equation (2.14) since the data of Shook et al. (2002) were limited to sand slurries. With the results of the current study, the range of particle densities has been expanded to include alumina (3950 kg/m³) and petroleum coke (1600 kg/m³) in addition to the large database for sand (2650 kg/m³). The good agreement between experimental data and the correlation shown in Figure 4.7 confirms the usefulness of the approach suggested by Shook and coworkers. With the expanded database resulting from the current study, it has been possible to replace the correlation of Equation (2.15) with the one presented here as Equation (4.2).

The correlation presented in Equation (4.2) applies only to the edge of the database. For $d^+ > 60$, experiments become difficult due to the increased Coulombic friction. To measure these values, vertical loops could be used.

It is of interest to note the difference between the formulation of the Shook correlation of Equation (2.15) and the correlation of Equation (4.2). The Shook correlation has an exponential term involving d^+ which is added to a constant of 0.00005. The new correlation subtracts a d^+ term from a larger constant of either 0.00042 or 0.00026. The Shook correlation incrementally adds less friction as d^+ increases whereas the new correlation subtracts more friction as d^+ increases. This subtraction can be seen as a reduction in the particle dispersive stress due to greater influence of near wall lift.

4.3 Alternate Methods for Determining C_∞

4.3.1 Concentric Cylinder Viscometer Tests

Slurries of each particle type were tested in the viscometer at four different concentrations. This was done to compare the behavior of the slurries in the pipeline and the viscometer and help determine the correct values for C_∞ for each set of particles. All experimental data are tabulated in Appendix B.

Schaan (2001) presented a relationship to predict the relative viscosity of a slurry, μ_r , from the concentration, C , and maximum packing concentration, C_∞ :

$$\mu_r = 1 + 2.5C + 0.16\lambda^2 \quad (4.3)$$

where

$$\lambda = \left[\left(\frac{C_\infty}{C} \right)^{1/3} - 1 \right]^{-1} \quad (4.4)$$

This correlation was developed from data collected at the SRC Pipe Flow Technology Centre for angular sand, rounded sand, and glass beads.

The data collected here were compared to the predictions of Schaan's correlation, Equation (4.3). The value of C_∞ for each slurry was chosen by modifying C_∞ until agreement was found with the majority of experimental data points. An example of this method can be seen in Figure 4.8, which presents data for aluminum oxide slurries:

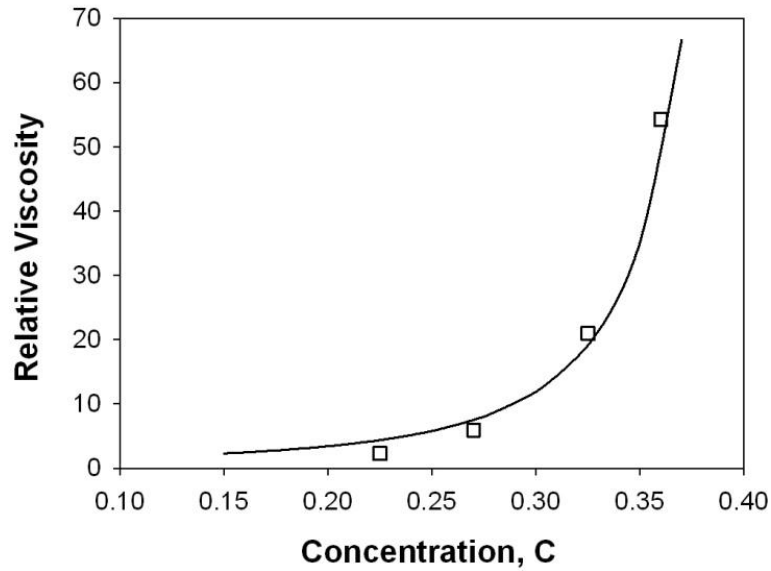


Figure 4.8 Schaan's correlation (solid line) and experimental data points for concentric cylinder viscometer tests of aluminum oxide slurries

The values determined using the Schaan correlation are presented in Table 4.3.

Table 4.3 Maximum packing concentration values determined from the Schaan correlation

Particles	C_{∞} from Viscometer
Aluminum Oxide	0.43
Angular Sand	0.50
Silica Flour	0.49
Petroleum Coke	0.64

The Schaan correlation appears to provide accurate predictions of C_{∞} (compared to the pipeline values) for the angular sand particles; however, the agreement is poor for the other particles. The comparison of C_{∞} values from the various techniques is presented in Table 4.5.

It is clear that the predictions for C_{∞} from the current concentric cylinder viscometer method are not accurate enough to be used as a substitute for pipeline tests.

4.3.2 Settling Tests

Settling tests were performed on the four particle types to measure C_{∞} . These tests were performed using the procedure outlined in section 3.3.4. The values found for maximum packing concentration from the settling method are presented in Table 4.4.

Table 4.4 Maximum packing concentration values determined from settling tests

Particles	C_{∞} from Settling
Aluminum Oxide	0.51
Angular Sand	0.53
Silica Flour	0.46
Petroleum Coke	0.61

For flow to take place, a settled bed of particles has to expand to the point where the particles begin to move by each other. This effect is illustrated in Table 4.5 where, for the majority of the particles, the C_{∞} values inferred from the pipe flow data are less than the settled bed concentrations. During the settling tests, the particles were able to settle to concentrations exceeding those at which the resistance to flow would have become nearly infinite.

The silica flour shows the opposite effect with C_{∞} inferred from the pipe flow data exceeding the settled bed concentration by a considerable amount. Perhaps

in this case, the colloidal-sized particles flocculate which would cause the volume occupied by particles to increase leading to an under-prediction of C_{∞} . This same phenomenon might not occur in the pipe loop tests due to the high shear environment inhibiting flocculation. This is an important discovery with significant impact on the design of slurry pipelines for the transport of relatively fine settling particles and should be studied further to determine the underlying cause.

4.3.3 Predictions of C_{∞} using the Hoffmann & Finkers' correlation

The maximum packing concentration, C_{∞} , was also calculated for each particle type using the Hoffmann & Finkers' correlation and the results are presented in Table 4.5 along with the C_{∞} values determined from pipeline, viscometer and settling tests.

Table 4.5 C_{∞} values found using different methods

Particles	C_{∞}			
	Pipeline	Viscometer	Hoffmann and Finkers' Correlation	Settling
Aluminum Oxide	0.48	0.43	0.46	0.51
Angular Sand	0.50	0.50	0.50	0.53
Silica Flour	0.62	0.49	N/A	0.46
Petroleum Coke	0.57	0.64	0.58	0.61

The Hoffmann-Finkers' correlation gives reasonable estimates of C_{∞} for all particles tested here. It is also notable that the correlation was developed from fluidized bed tests and not pipeline data. The fact that the correlation agrees well

for the particles studied here is promising but it is still a very small sample set and this should be taken into consideration if this method is used.

4.3.4 Summary of Methods

The frictional pressure gradient for the 30% aluminum oxide slurry flowing in the 75 mm pipe loop is presented in Figure 4.9 as an illustration of the accuracy of each method in predicting the pipeline C_∞ value. The experimental data acquired from the pipeline experiments are compared with the predictions obtained when C_∞ values from the viscometer method, settling method, and the Hoffmann-Finkers' correlation are used in the f_s correlation.

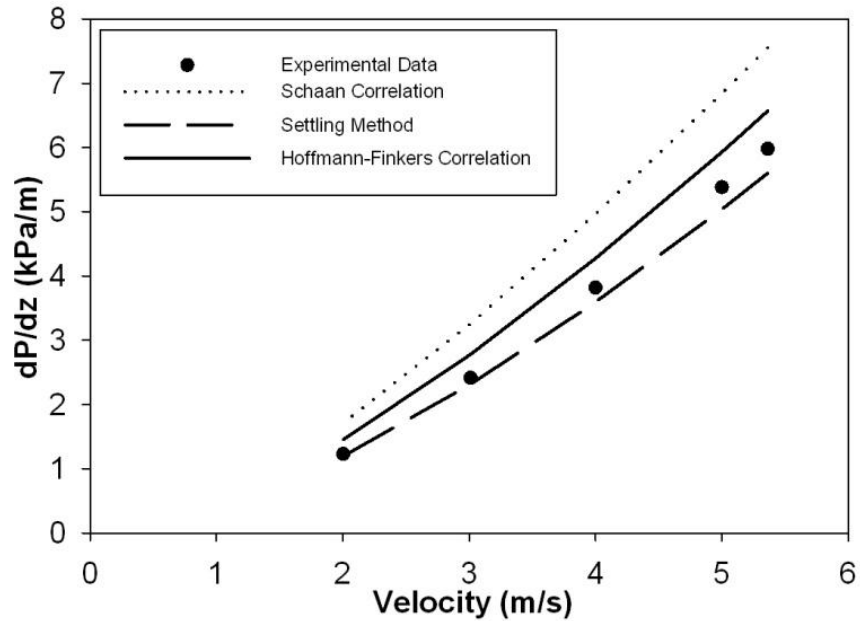


Figure 4.9 Friction loss predictions for an aluminum oxide slurry (30% solids by volume) in a 75 mm pipeline loop. Predictions shown here based on the different methods for prediction C_{∞} . Actual pipeline data shown for comparison.

The dangers of using an incorrect value for C_{∞} predicting pipeline friction losses and/or deposition velocity must be considered. For example, the C_{∞} values obtained from the viscometer and pipeline tests of the petroleum coke were 0.64 and 0.57, respectively. The difference is illustrated in the following Table 4.6, which shows the effect of C_{∞} on predictions of the pipeline deposition velocity (V_c) for a petroleum coke slurry (30% solids by volume).

Table 4.6 Comparison of methods for determining C_∞ for petroleum coke

Method for Determination of C_∞	C_∞	Predicted V_c (m/s)
Pipeline Tests	0.57	0.8
Viscometer Tests	0.64	0.7

Using the 2007 SRC Pipeflow model [Sanders et al. (2004), and Gillies et al. (2004)] to model a 75 mm diameter pipeline at a concentration of 30% petroleum coke by volume in water at 20°C gives the deposition velocities shown in Table 4.6. This difference would become more pronounced if the concentration were increased. Friction loss predictions also depend on C_∞ , and the discrepancy associated with these C_∞ values would increase as the concentration increases. In this case, trusting the results of the viscometer method would result in an over-prediction in C_∞ , producing an under-prediction in the settling velocity. This could ultimately lead to settling in the pipeline and blockages.

The reverse could also occur, as seen with results of the settling tests for silica flour. The C_∞ value predicted by the settling method was 0.46 while the value obtained from the pipeline data was 0.62. If one were to model a system using the results of the settling method, C_∞ would be greatly under-predicted. This would result in a design which requires a higher minimum operating velocity than is actually necessary. The energy wasted on maintaining this higher velocity would result in higher operating costs.

It is recommended that when C_∞ must be determined, pipeline tests should be considered first. If pipeline tests are not possible, then one could consider batch settling tests, provided that the particle size distribution is relatively narrow and the particles are not colloidal in size. The Hoffmann-Finkers correlation could also be used as an estimate for C_∞ ; however, additional experiments comparing the correlation to pipeline data should be conducted to determine the true validity of the method. The Schaan correlation appears to predict a value for C_∞ that is dissimilar from the pipeline-based value, for all particles except angular sand. Also, the selection of the appropriate relative viscosity-concentration equation is not obvious. The Schaan correlation does not seem to be appropriate for predicting C_∞ except for angular sand.

It is clear from these tests that in order to get a true value for C_∞ of a certain particle type, pipeline tests should be used. One must remember with other methods some degree of error should be expected; and one should design with this error in mind to ensure a reliable operation.

4.4 Bimodal distributions of different particle types

Data were also collected for slurries containing various concentrations of sand and alumina together. The collected data needed to be analyzed differently in an attempt to apply the f_s correlation presented in Section 4.2. Recall that the correlation requires a value for d^+ , which is calculated using the mass median particle diameter: for the bimodal slurries, there are two different median diameters in the system. Also, one value of C_∞ must be used in the correlation;

however, there are two different particle types. It was decided that an average value of 0.49 would be used for the sand/alumina mixture since the individual C_{∞} values are 0.50 and 0.48, respectively. Additionally, the particle sizes are similar and thus one particle type could not occupy the interstices within the close-packed structure of the other particle type. An average diameter was calculated at each concentration in order to use both particle diameters. These average diameters were the average diameter of the specific particle types weighted by their volume fractions in the system. For example, data were taken with a slurry of 18.3% by volume aluminum oxide and 8.3% by volume angular sand. The calculation for determining the average diameter was as follows:

$$\begin{aligned}
 x_{A,overall} &= 0.183 \\
 x_{S,overall} &= 0.083 \\
 x_{A,solids} &= \frac{x_{A,overall}}{x_{A,overall} + x_{S,overall}} = \frac{0.183}{0.183 + 0.083} = 0.688
 \end{aligned}$$

$$\begin{aligned}
 d_{avg} &= d_A x_{A,solids} + d_S x_{S,solids} \\
 d_{avg} &= 67.0 \mu m (0.688) + 104 \mu m (0.312) = 78.5 \mu m
 \end{aligned}$$

By calculating d^+ using this average diameter, the existing correlation provides excellent predictions:

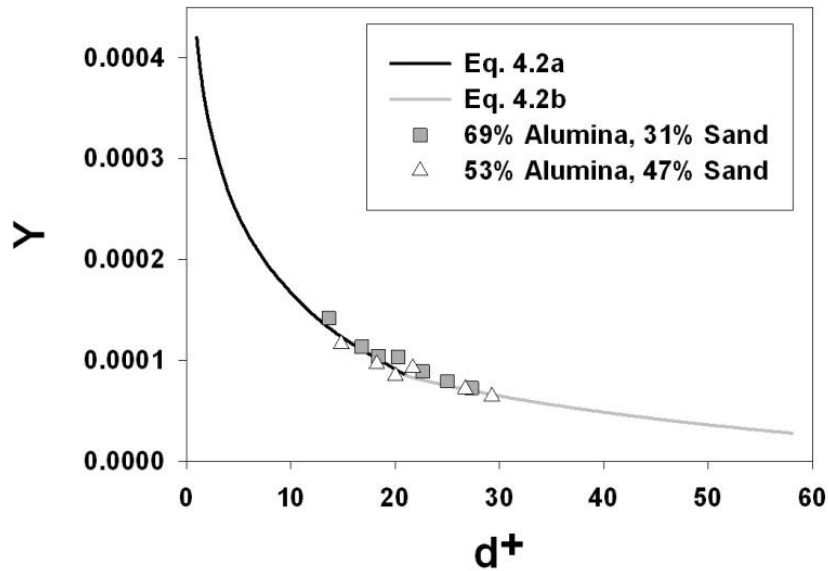


Figure 4.10 Bimodal particle slurries compared with the kinematic friction correlation for single particle slurries

It can be seen that the data, when analyzed using volume fraction averaging, are modeled accurately with the kinematic friction correlation. However, the range of d^+ values studied here is in a narrow and rather flat portion of the f_s curve. In fact, the volume-weighted averaging for the particle diameter was chosen arbitrarily and a mass-weighted averaging fits with similar agreement due to the linearity of this portion of the curve. Future work needs to be conducted with higher viscosity carrier fluids to model the low d^+ portion of the curve and with larger particle sizes to model the high d^+ portion of the curve. It would be beneficial to test vastly different particle types to determine the correct diameter-averaging method to be used.

5 CONCLUSIONS AND RECOMMENDATIONS

Two different studies were performed in this research: pipeline experiments to determine a correlation to predict the particle friction factor, f_s , for slurries of varied particle sizes and densities, and different methods for determining the maximum particle concentration, C_∞ , were studied and compared.

Pressure gradients were obtained as a function of velocity for different concentrations of slurries of each particle type. The Shook correlation, Equation (2.14), was used as a starting point for analyzing the data. This correlation was developed using sand slurry data. In this study, it was found that a logarithmic correlation best fit the data, and a new correlation for f_s was created, shown here as Equation (4.2). This correlation covers a wider range of particle densities and diameters than the original correlation (Equation 2.14).

$$Y = \frac{f_s}{\lambda^{1.25}} = A \ln(d^+) + B \quad (4.2)$$

where for $d^+ \leq 21$:

$$A = -1.1 \times 10^{-4} \text{ and } B = 4.2 \times 10^{-4} \quad (4.2a)$$

For $d^+ > 21$:

$$A = -5.6 \times 10^{-5} \text{ and } B = 2.6 \times 10^{-4} \quad (4.2b)$$

Methods for determining C_∞ for use in pipe flows were studied and compared. The Schaan correlation (Equation 4.3) was developed previously as a viscometer-based method, and was found to be unsatisfactory due to the inaccurate predictions of C_∞ when studying any particle type other than sand.

The settling method produces reasonable estimates of C_∞ for particles of narrow size distributions. The method fails, however, if colloidal-sized particles are present. The reason for this discrepancy has not been studied here but future work should be performed to explore this discovery.

The Hoffmann-Finkers correlation provided good estimates for C_∞ ; as well, it can be used when the particle size distribution is broad. However, the range of applicability of this method is not certain as it has only been tested on the particle types studied here. It is recommended that additional pipeline experiments be conducted over a much broader range of conditions.

For friction loss predictions, the value of C_∞ obtained from pipeline tests is most accurate. One must remember with other methods some degree of error should be expected. One should design with this error in mind to ensure a safe operation.

A few pipeline tests of bimodal slurries containing aluminum oxide and angular sand conducted as part of a preliminary attempt to model multi-particle slurries of interest in the hard-rock mining industry. By using a volume-averaged particle diameter, the experimental data fit the new f_s correlation very well. This result is promising; however future work must be performed to study a much broader range of conditions.

The correlation in Equation (4.2) is best when applied to narrowly sized particles where the effects can be captured reasonably well using an average particle size. The correlation is limited by the dimensionless particle diameters studied. It is recommended that work be performed in vertical pipe loops where Coulombic friction will not be a factor in order to extend the database and correlation. More work needs to be performed to expand the method for more complex slurries containing particles with broad or multimodal size distributions. Also work should be done to determine how best to deal with slurries containing different species of particles with multiple densities.

6 REFERENCES

Bagnold, R.A., "Experiments on a Gravity-Free Dispersion of Large Solid Spheres in a Newtonian Fluid Under Shear", Proc. Roy. Soc., London, Ser. A, Vol. 225, 49-63 (1954).

Churchill, S.W., "Friction Factor Equation Spans All Fluid Regimes," Chem. Eng. **84** (24): 91-92. (1977).

Clift, R., J.R. Grace and M.E. Weber, *Bubbles, Drops and Particles*, Academic press, New York (1978).

Durand, R. and Condolios, E., "Experimental Study of the Hydraulic Transport of Coal and Solid Materials in Pipes", Proc. Colloq. On the Hydraulic Transport of Coal, Nat. Coal Board, U.K., Paper IV, 39-55 (1952).

Gillies, R.G., Pipeline Flow of Coarse Particle Slurries. *University of Saskatchewan: Ph.D. Thesis, Dept. of Chemical Engineering* (1993).

Gillies, R.G., *Pipeline Flow of Settling Slurries: A Summary of Recent Innovations*. SRC Publication No. 11606-1E03, (2003).

Gillies, R.G., K.B. Hill, M.J. McKibben, and C.A. Shook, "Sand Transport by Newtonian Fluids in Laminar Pipe Flow", *Powder Technology* **104**, 269-277 (1999).

Gillies, R.G., J. Schaan, R.J. Sumner, M.J. McKibben, and C.A. Shook, "Deposition Velocities for Newtonian Slurries in Turbulent Flow", *Can. J. Chem. Eng.* **78**, 704-708 (2000).

Gillies, R.G. and C.A. Shook, "Concentration Distributions of Sand Slurries in Horizontal Pipe Flow", *Part. Sci. Tech.* **12**, 45-69 (1994).

Gillies, R.G. and C.A. Shook, "Modelling High Concentration Settling Slurry Flows", *Can. J. Chem. Eng.* **78**, 709-716 (2000).

Gillies, R.G., C.A. Shook, and K.C. Wilson, "An Improved Two-Layer Model for Horizontal Slurry Pipeline Flow", *Can. J. Chem. Eng.* **69**, 173-179 (1991).

Gillies, R.G., C.A. Shook and J. Xu, "Modelling Heterogeneous Slurry flows at High Velocities", *Can. J. Chem. Eng.* **82**, 1060-1065 (2004).

Hoffmann, A.C. and H.J. Finkers, A Relation for the Void Fraction of Randomly Packed Particle Beds. *Powder Technology* **82**, 197-203 (1995).

Perry, R.H., *Perry's Chemical Engineers' Handbook Fourth Edition*. McGraw-Hill Book Company, 5-60 (1963).

Saffman, P.G., "The Lift on a Small Sphere in a Low Shear Flow", *J. Fluid Mech.*, Vol. 22, 385-400 (1965).

Sanders, R.S., R. Sun, R.G. Gillies, M.J. McKibben, C. Litzenberger, C.A. Shook, Deposition Velocities for Particles of Intermediate Size in Turbulent Flow, *Proc. Hydrotransport 16*, BHR Group, Cranfield, U.K., 429-442, (2004).

Schaan, J.J., Pipeline Flow of Newtonian Fine Particle Slurries. *University of Saskatchewan: M.Sc. Thesis, Dept. of Chemical Engineering* (2001).

Schaan, J. and C.A. Shook, "Anomalous Friction in Slurry Flows", *Can. J. Chem. Eng.* **78**, 726-730 (2000).

Schaan, J., R.J. Sumner, R.G. Gillies, and C.A. Shook, "The Effect of Particle Shape on Pipeline Friction for Newtonian Slurries of Fine Particles", *Can J. Chem. Eng.* **78**, 717-725 (2000).

Shook, C.A. and A.S. Bartosik, "The Pseudohomogeneous Flow Approximation for Dispersed Two-Phase Systems", *Particulate Science and Technology*, Vol. 9, 119-134 (1991).

Shook, C.A., L. Geller, R.G. Gillies, W.H.W. Husband, and M. Small, "Experiments with Coarse Particles in a 250 mm Pipeline", *Proc. Hydrotransport 10*, BHR Group, Cranfield, U.K., 219-227, 1986.

Shook, C.A., R.G. Gillies, and R.S. Sanders, *Pipeline Hydrotransport with Applications in the Oil Sand Industry*, Saskatchewan Research Council, Saskatoon, Canada, SRC Publication 11508-1E02 (2002).

Shook, C.A., R.G. Gillies and J. Xu, "Modelling Heterogeneous Slurry Flows at High Velocities", *Can J. Ch. E.*, Vol 82. No. 5, 1060-1065 (2004).

Shook, C.A. and M.C. Roco, *Slurry Flow Principles and Practice*, Butterworth-Heinemann 1-5, 219-221 (1991).

Singh, S.N., V. Seshadri, R. Mishra, and C. Fabien, Settled Bed Characteristics in a Multisized Particulate Solid-Liquid Suspension. *Powder Handling & Processing* **13**, 191-196 (2001).

Spells, K.E., “Correlations for Use in Transport of Aqueous Suspensions of Fine Solids Through Pipes”, *Trans. Inst. Chem. Eng.*, **33**, 79-84 (1955).

Thomas, D.G., “Transport Characteristics of Suspensions: VIII. A Note on the Viscosity of Newtonian Suspensions of Uniform Spherical Particles. *J. Colloid Sci.* **20**: 267-277. (1965).

Wasp, E.J., Aude, T.C., Kenny, J.P. and Williams, P.B., “Deposition Velocities, Transition Velocities and Spatial Distribution of Solids in Slurry Pipelines”, *Proc. Hydrotransport 1*, BHRA Fluid Engineering, Cranfield U.K., Paper H4, 53-76 (1970).

Wilson, K.C., “A Unified Physically Based Analysis of Solid Liquid Pipeline Flow,” *Proc. 4th Int. Conf. on the Hydraulic Transport of Solids in Pipes*, BHRA Fluid Engineering, Cranfield, U.K., Paper A1, 1-16 (1976).

Wilson, K.C., R.S. Sanders, R.G. Gillies and C.A. Shook, “Verification of the Near-wall Model for Slurry Flow”, *Powder Technology*, Vol. 197, 247-253 (2010).

Wilson, K.C., and A. Sellgren, “Revised Method for Calculating Stratification Ratios for Heterogeneous Slurry Flows”, *Proc. 14th Conf. on Transport and Sedimentation of Solid Particles*, St. Petersburg, Russia (2008).

SYMBOLS

a	absorption coefficient
c	local concentration, volume fraction
C	solids concentration, volume fraction
C_{∞}	maximum particle concentration, volume fraction
C_D	drag coefficient for a particle settling at its terminal velocity, dimensionless
d	particle diameter (μm)
d_{50}	median particle diameter (μm)
d^+	dimensionless particle diameter (Equation 2.16)
D	diameter of a pipeline (m)
f	Fanning friction factor (Equation 2.2)
F_{lift}	lift force acting on a particle (N)
g	acceleration due to gravity (m/s^2)
h	height above a datum (m)
L	length of viscometer spindle or length of chord in pipe (m)
N	intensity of a beam observed through a medium (W/sr)

N_0	unattenuated beam intensity (W/sr)
P	Pressure (Pa)
R	radius of viscometer spindle or cup (m)
Re	Reynolds number (Equation 2.4, Equation 2.6)
S	specific gravity
T	torque measured from viscometer spindle (N·m)
u^*	friction velocity (m/s)
v_∞	single particle terminal settling velocity (m/s)
V	bulk velocity (m/s)
V_c	deposition velocity (m/s)
V_c^*	dimensionless deposition velocity (Equation 2.10)
x	volume fraction of a particle type in a bimodal slurry or path length in pipe
y	distance from bottom of pipe (m)
Y	used in place of $f_s \lambda^{-1.25}$ in some equations and plots
z	horizontal distance in pipeline (m)

Greek Symbols

$\dot{\gamma}$ shear rate (s^{-1})

ε void fraction

λ linear solids concentration (Equation 2.9)

μ Newtonian viscosity ($\text{Pa}\cdot\text{s}$)

ρ density (kg/m^3)

ρ^* dimensionless density

σ standard deviation of the particle size distribution

τ_w wall shear stress of mixture (Pa)

$\tau_{w,f}$ wall shear stress of carrier fluid (Pa)

τ_k kinematic contribution to wall shear stress (Pa)

ϕ excess friction loss term

φ sphericity of a particle

ω rotational spindle speed (radians/s)

Subscripts

avg denotes average (mean)

f denotes carrier fluid

m denotes mixture, or slurry

p particle (as in particle Reynolds number)

r relative (ratio of slurry viscosity to carrier fluid viscosity, for example)

s denotes solids

APPENDICES

Appendix A: Particle Size Distributions

Aluminum Oxide		
Particle Diameter (μm)	Fraction Retained	Cumulative Fraction Retained
106	0.000	0.000
75	0.352	0.352
53	0.398	0.750
45	0.149	0.899
32	0.025	0.924
26	0.025	0.950
22	0.025	0.975
18	0.025	1.000

Angular Sand		
Particle Diameter (μm)	Fraction Retained	Cumulative Fraction Retained
300	0.000	0.000
212	0.099	0.099
150	0.088	0.187
106	0.280	0.466
75	0.446	0.912
53	0.045	0.957
45	0.025	0.982
32	0.018	1.000

Silica Flour		
Particle Diameter (μm)	Fraction Retained	Cumulative Fraction Retained
53	0.000	0.000
42	0.249	0.249
29	0.193	0.442
21	0.159	0.601
17	0.124	0.725
14	0.092	0.817
10	0.080	0.897
7	0.057	0.954
5	0.023	0.977
3	0.023	1.000

Petroleum Coke		
Particle Diameter (μm)	Fraction Retained	Cumulative Fraction Retained
300	0.000	0.000
212	0.112	0.112
150	0.262	0.375
106	0.304	0.678
75	0.226	0.904
53	0.051	0.955
45	0.018	0.972
32	0.028	1.000

Appendix B: Viscometer Sample Calculation and Data

Sample Calculation

The calculation of the relative viscosity of a slurry of 22.5% aluminum oxide in a glycol-glycerol mixture is presented here. The first step was to determine the carrier fluid viscosity. A mixture of 75% glycerol and 25% glycol was used as the carrier fluid and these tests were performed at 22.5°C. The dimensions of the concentric cylinder viscometer are presented in Table B.1.

Table B.1: Concentric cylinder viscometer dimensions

Spindle Type	MV2
Length of Spindle, L	0.060 m
Outer Radius of Spindle, R_1	0.0184 m
Inner Radius of Cup, R_2	0.0210 m

The software accompanying the viscometer recorded the rotational speed of the spindle and the consequent torque. The data were collected at increasing speeds from 5 RPM to 40 RPM in four steps and then at decreasing speeds to 5 RPM in the same number of steps. The reason for this procedure was to monitor the data for any apparent non-Newtonian behavior such as Taylor vortices or incomplete shear in these slurries that were known to be Newtonian. The data for the carrier fluid are presented in Table B.2.

Table B.2: Glycerol-glycol mixture experimental data at 22.5°C

w (1/min)	T (μNM)
5.0	404
16.6	1314
28.3	2230
40.0	3145
40.0	3149
28.3	2235
16.6	1317
5.0	396

The integrated equation for concentric cylinder viscometry of a Newtonian fluid is:

$$\omega = \frac{T}{4\pi L\mu} \left[\frac{1}{R_1^2} - \frac{1}{R_2^2} \right] \quad (\text{B.1})$$

where ω is the rotational speed converted to radians/s. A plot of T/L as a function of ω will allow determination of the viscosity.

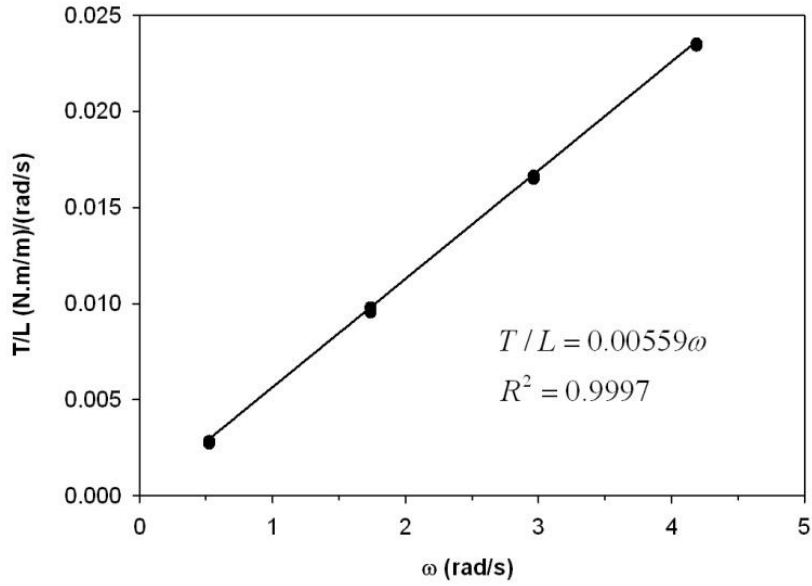


Figure B.1: Glycerol-glycol mixture viscometer measurements at 22.5°C

The viscosity can then be determined by solving for μ in Equation (B.1) using the slope of the best fit line found in the plot. In this example, the carrier fluid viscosity was determined to be 305 mPa·s.

The next step in the procedure was to measure the slurry viscosity. A slurry of 22.5% aluminum oxide in this glycerol-glycol carrier fluid was tested in the viscometer with the same procedure at the same temperature. The experimental data results for this test are presented in Table B.3.

Table B.3: 22.5% aluminum oxide in glycerol-glycol experimental data at
22.5°C

w (1/min)	T (μNM)
5.0	404
16.6	1314
28.3	2230
40.0	3145
40.0	3149
28.3	2235
16.6	1317
5.0	396

From these data

$$\mu_m = 685 \text{ mPa} \cdot \text{s}$$

$$\mu_r = \frac{685 \text{ mPa} \cdot \text{s}}{305 \text{ mPa} \cdot \text{s}} = 2.25$$

Viscometer Data

Material: Aluminum
Oxide

Concentration	Temperature (°C)	Slurry Viscosity (mPa·s)	Carrier Fluid Viscosity (mPa·s)	Relative Viscosity
0.225	22.5	685	305	2.25
0.270	22.5	1577	291	5.42
0.325	22.5	4957	298	16.64
0.360	22.5	12625	331	38.17

Material: Angular
Sand

Concentration	Temperature (°C)	Slurry Viscosity (mPa·s)	Carrier Fluid Viscosity (mPa·s)	Relative Viscosity
0.225	22.5	834	318	2.62
0.270	23.0	1290	296	4.36
0.325	22.0	2413	315	7.67
0.360	22.5	5713	307	18.63

Material: Petroleum
Coke

Concentration	Temperature (°C)	Slurry Viscosity (mPa·s)	Carrier Fluid Viscosity (mPa·s)	Relative Viscosity
0.225	22.5	636	324	1.96
0.270	22.5	863	307	2.80
0.325	23.0	1226	307	4.00
0.360	24.0	1741	290	6.00

Material: Silica Flour

Concentration	Temperature (°C)	Slurry Viscosity (mPa·s)	Carrier Fluid Viscosity (mPa·s)	Relative Viscosity
0.20	23.0	498	199	2.50
0.30	23.0	1306	199	6.56
0.35	24.0	2332	185	12.62
0.40	24.0	6098	185	33.02

Material: 69% Alumina 31% Sand

Concentration	Temperature (°C)	Slurry Viscosity (mPa·s)	Carrier Fluid Viscosity (mPa·s)	Relative Viscosity
0.225	22.5	848	300	2.83
0.266	22.5	1615	343	4.71
0.325	22.5	3824	307	12.45
0.370	23.0	10505	297	35.40

Material: 53% Aluminum Oxide 47% Sand

Concentration	Temperature (°C)	Slurry Viscosity (mPa·s)	Carrier Fluid Viscosity (mPa·s)	Relative Viscosity
0.225	23.0	770	334	2.30
0.266	23.0	1248	322	3.87
0.325	23.5	3533	309	11.43
0.370	23.5	9627	308	31.25

Appendix C: Experimental Pipeline Pressure Gradients

Pipeline flow data for 92 micron sand (LM 125) in 158 mm diameter pipeline

Data collector: Jason Schaan
 Temp: 20°C
 Carrier: Water
 Pipe Diameter: 0.1585 m

Pipe Roughness: 15.0 μm
 Solids: 92 μm sand (LM 125)
 Solids C_{∞} : 0.50
 Solids Density: 2650 kg/m³

V (m/s)	dP/dz (kPa/m)	C
5.48	1.531	0.135
5.02	1.305	0.135
4.51	1.077	0.135
4.01	0.875	0.135
3.49	0.687	0.135
5.53	1.967	0.267
4.99	1.676	0.267
4.53	1.426	0.267
3.99	1.149	0.267
3.49	0.912	0.267
4.97	2.062	0.307
4.51	1.721	0.307

V (m/s)	dP/dz (kPa/m)	C
4.02	1.423	0.307
3.52	1.145	0.307
4.01	1.603	0.326
3.52	1.276	0.326
3.98	1.883	0.354
3.47	1.511	0.354
5.46	1.648	0.267
4.99	1.354	0.267
4.53	1.157	0.267
4.01	0.943	0.267
3.50	0.751	0.267

Pipeline flow data for 92 micron sand (LM 125) in 52 mm diameter pipeline

Data collector: Jason Schaan
 Temp: 20°C
 Carrier: Water
 Pipe Diameter: 0.0521 m

Pipe Roughness: 1.0 μm
 Solids: 92 μm sand (LM 125)
 Solids C_{∞} : 0.50
 Solids Density: 2650 kg/m³

V (m/s)	dP/dz (kPa/m)	C
5.00	4.227	0.145
4.50	3.530	0.145
4.00	2.896	0.145
3.50	2.306	0.145
3.00	1.785	0.145
4.95	5.793	0.291
4.50	4.989	0.291
4.00	4.144	0.291

V (m/s)	dP/dz (kPa/m)	C
3.50	3.349	0.291
3.00	2.612	0.291
4.98	7.198	0.339
4.51	6.146	0.339
3.99	5.068	0.339
3.49	4.065	0.339
3.00	3.169	0.339

Pipeline flow data for 90 micron sand in 102.7 mm diameter pipeline

Data collector: Jihuai Xu
 Temp: 20°C
 Carrier: Water
 Pipe Diameter: 0.1027 m

Pipe Roughness: 2.0 μm
 Solids: 90 μm sand
 Solids C_{∞} : 0.50
 Solids Density: 2650 kg/m³

V (m/s)	dP/dz (kPa/m)	C
7.76	4.387	0.190
7.02	3.642	0.190
5.95	2.699	0.190
4.88	1.889	0.190
3.85	1.267	0.190
7.72	4.609	0.238
6.99	3.850	0.238
5.88	2.836	0.238
4.83	2.058	0.238
3.93	1.453	0.238

V (m/s)	dP/dz (kPa/m)	C
7.47	4.775	0.284
6.97	4.194	0.284
5.98	3.249	0.284
4.99	2.329	0.284
3.90	1.563	0.284
7.17	5.314	0.332
6.53	4.512	0.332
5.81	3.732	0.332
4.96	2.899	0.332
3.79	1.834	0.332

Pipeline flow data for 86 micron sand in 102.7 mm diameter pipeline

Data collector: SRC Report
Temp: 20°C
Carrier: Glycol
Pipe Diameter: 0.1027 m

Pipe Roughness: 5.0 μm
Solids: 86 μm sand
Solids C_{∞} : 0.56
Solids Density: 2650 kg/m^3

V (m/s)	dP/dz (kPa/m)	C
2.50	0.899	0.149
2.11	0.667	0.149
2.50	0.984	0.149
2.10	0.721	0.149
2.50	1.039	0.149
2.10	0.766	0.149
2.50	1.086	0.149
2.10	0.801	0.149
2.50	1.082	0.234
2.10	0.796	0.234

V (m/s)	dP/dz (kPa/m)	C
2.50	1.194	0.234
2.10	0.885	0.234
2.50	1.274	0.237
2.10	0.943	0.237
2.50	1.217	0.304
2.10	0.902	0.304
2.50	1.340	0.305
2.10	0.995	0.305
2.50	1.584	0.305
2.10	1.138	0.305

Pipeline flow data for 67 micron aluminum oxide in 75.4 mm diameter pipeline

Data collector: Dan Gillies
 Date: June 2009
 Temp: 20°C/40°C
 Carrier: Water

Pipe Diameter: 0.0754 m
 Pipe Roughness: 6.0 μm
 Solids: 67 μm aluminum oxide
 Solids C_{∞} : 0.48
 Solids Density: 3950 kg/m^3

Temperature: 20°C		
V (m/s)	dP/dz (kPa/m)	C
6.79	6.062	0.193
6.00	4.985	0.193
5.00	3.725	0.193
4.01	2.632	0.193
5.36	5.977	0.301
5.00	5.379	0.301
4.00	3.815	0.301
3.98	5.272	0.378
3.48	4.475	0.378

Temperature: 40°C		
V (m/s)	dP/dz (kPa/m)	C
6.84	5.295	0.193
5.99	4.246	0.193
5.00	3.118	0.193
4.01	2.220	0.193
5.63	5.463	0.301
5.00	4.575	0.301
4.01	3.299	0.301
4.00	4.122	0.373
3.50	3.358	0.373

Pipeline flow data for 131 micron Syncrude coke in 75.6 mm diameter pipeline

Data collector: Dan Gillies
 Date: October 2009
 Temp: 20°C/40°C
 Carrier: Water

Pipe Diameter: 0.0756 m
 Pipe Roughness: 4.0 μm
 Solids: 131 μm coke
 Solids C_{∞} : 0.57
 Solids Density: 1600 kg/m^3

Temperature: 20°C		
V (m/s)	dP/dz (kPa/m)	C
7.03	4.778	0.188
6.03	3.664	0.188
5.03	2.666	0.188
7.04	5.012	0.298
6.03	3.876	0.298
5.03	2.858	0.298
6.58	4.435	0.368
6.05	3.902	0.368
5.03	2.910	0.368

Temperature: 40°C		
V (m/s)	dP/dz (kPa/m)	C
7.02	4.416	0.191
5.97	3.278	0.191
4.99	2.389	0.191
7.03	4.462	0.299
6.04	3.436	0.299
5.01	2.496	0.299
6.56	5.259	0.390
6.05	4.616	0.390
5.03	3.457	0.390

Pipeline flow data for 28 μm silica flour in 75.6 mm diameter pipeline

Data collector: Dan Gillies
 Date: July 2008
 Temp: 25°C/50°C
 Carrier: Water

Pipe Diameter: 0.0753 m
 Pipe Roughness: 0.0 μm
 Solids: 28 μm silica flour
 Solids C_{∞} : 0.62
 Solids Density: 2660 kg/m^3

Temperature: 25°C		
V (m/s)	dP/dz (kPa/m)	C
6.99	5.835	0.207
6.00	4.472	0.207
4.99	3.271	0.207
3.99	2.214	0.207
2.99	1.351	0.207
2.00	0.664	0.207
6.99	7.183	0.291
6.02	5.537	0.291
5.00	4.018	0.291
3.99	2.768	0.291
3.00	1.711	0.291
2.01	0.860	0.291
6.59	8.052	0.352
6.01	6.819	0.352
5.00	4.983	0.352
4.00	3.413	0.352
3.00	2.077	0.352

Temperature: 25°C		
V (m/s)	dP/dz (kPa/m)	C
2.00	1.026	0.352
5.90	7.914	0.402
5.00	5.961	0.402
4.01	4.070	0.402
3.00	2.456	0.402
2.01	1.208	0.402
Temperature: 50°C		
V (m/s)	dP/dz (kPa/m)	C
6.66	7.668	0.393
6.00	6.370	0.393
4.99	4.694	0.393
3.99	3.175	0.393
3.01	1.964	0.393
2.01	0.977	0.393

Pipeline flow data for mixture of aluminum oxide and sand slurries in 75.39 mm pipeline

Data collector: Dan Gillies
 Date: June 2009
 Temp: 20°C/40°C
 Carrier: Water
 Pipe Diameter: 0.07539 m
 Pipe Roughness: 6.0 µm

Solids: 67.0 µm aluminum oxide and
 104.0 µm sand
 Solids C_{∞} : 0.50
 Solids Densities: aluminum oxide –
 3950 kg/m³, sand - 2650 kg/m³

Temperature: 20°C			
V (m/s)	dP/dz (kPa/m)	C aluminum	C sand
6.50	5.50	0.185	0.000
6.00	4.83	0.185	0.000
5.50	4.21	0.185	0.000
5.00	3.59	0.185	0.000
4.50	3.03	0.185	0.000
4.00	2.51	0.185	0.000
5.51	4.84	0.183	0.083
5.01	4.17	0.183	0.083
4.00	2.99	0.183	0.083
5.53	6.12	0.184	0.163
5.01	5.42	0.184	0.163
4.01	3.92	0.184	0.163

Temperature: 40°C			
V (m/s)	dP/dz (kPa/m)	C aluminum	C sand
6.53	4.85	0.185	0.000
6.02	4.22	0.185	0.000
5.03	3.12	0.185	0.000
4.02	2.16	0.185	0.000
5.51	4.06	0.181	0.082
5.01	3.48	0.181	0.082
4.51	2.96	0.181	0.082
4.01	2.50	0.181	0.082
5.52	5.07	0.182	0.161
5.01	4.42	0.182	0.161
4.01	3.27	0.182	0.161

Appendix D: Rejected Model Fits

This appendix shows the other methods attempted in correlating the experimental data. These methods were rejected because of the lower R^2 values.

In the plots below, $Y = f_s \lambda^{-1.25}$.

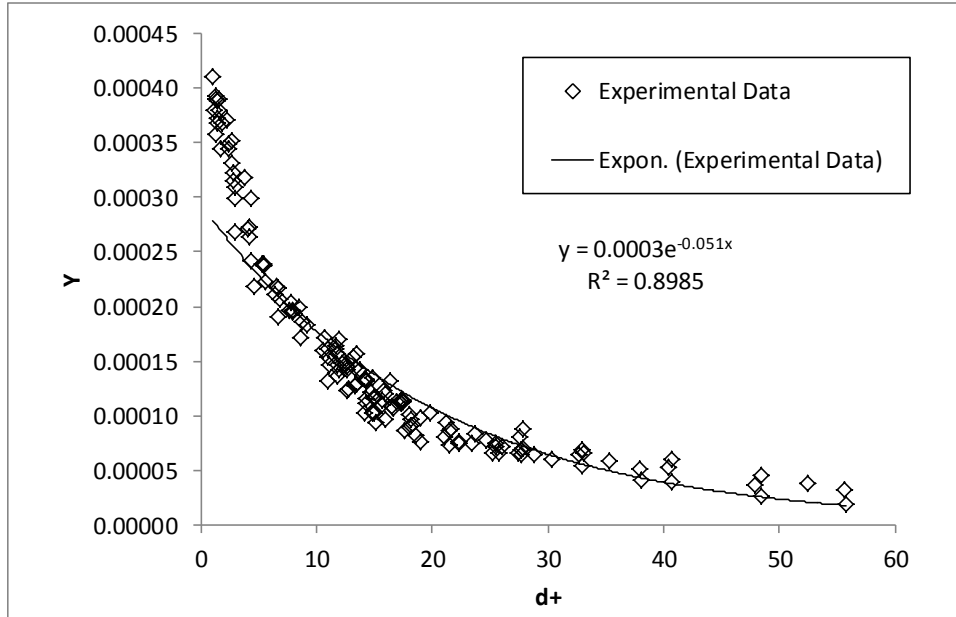


Figure D.1: Experimental data presented with an exponential fit

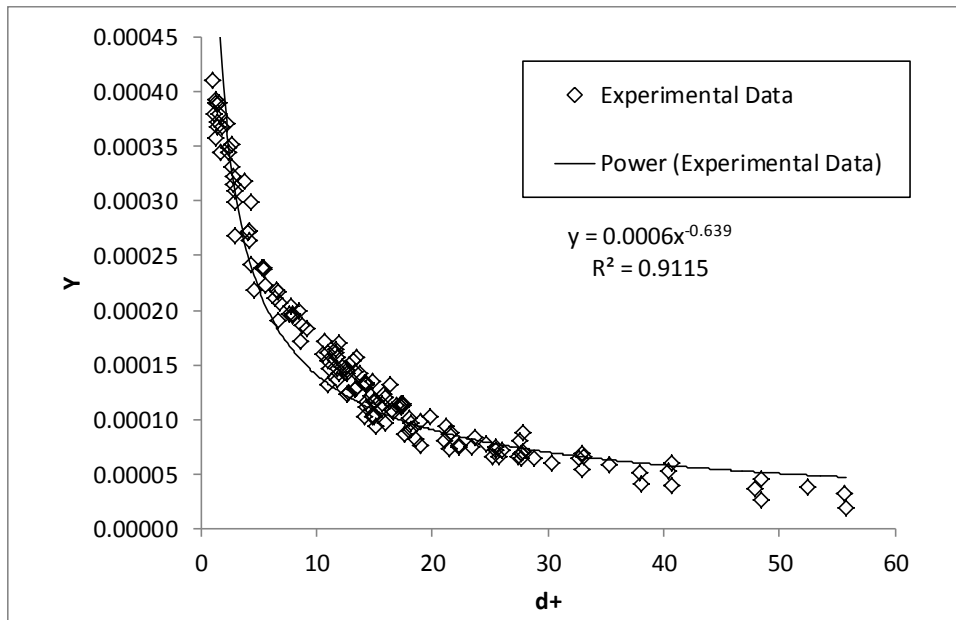


Figure D.2: Experimental data presented with a power fit